Disordered mesoscopic systems with interactions: induced two–body ensembles and the Hartree–Fock approach

Y. Alhassid,[1] H. A. Weidenmüller[2] and A. Wobst[3]
[1] *Center for Theoretical Physics, Sloane Physics Laboratory, Yale University, New Haven, CT 06520, USA*
[2] *Max-Planck-Institut für Kernphysik, D-69029 Heidelberg, Germany*
[3] *Institut für Physik, Universität Augsburg, 86135 Augsburg, Germany*

We introduce a generic approach to study interaction effects in diffusive or chaotic quantum dots in the Coulomb blockade regime. The randomness of the single–particle wave functions induces randomness in the two–body interaction matrix elements. We classify the possible induced two–body ensembles, both in the presence and absence of spin degrees of freedom. The ensembles depend on the underlying space–time symmetries as well as on features of the two–body interaction. Confining ourselves to spinless electrons, we then use the Hartree–Fock (HF) approximation to calculate HF single–particle energies and HF wave functions for many realizations of the ensemble. We study the statistical properties of the resulting one–body HF ensemble for a fixed number of electrons. In particular, we determine the statistics of the interaction matrix elements in the HF basis, of the HF single–particle energies (including the HF gap between the last occupied and the first empty HF level), and of the HF single–particle wave functions. We also study the addition of electrons, and in particular the distribution of the distance between successive conductance peaks and of the conductance peak heights.

PACS numbers: 73.23.Hk, 05.45.Mt, 73.63.Kv, 73.23.-b

I. INTRODUCTION

In this paper, we explore a generic approach to interaction effects in diffusive and/or chaotic quantum dots in the Coulomb blockade regime. To set the stage, we describe in this Introduction some previous work, and discuss the motivation of our own investigation.

Electron transport in quantum dots that are strongly coupled to leads (open dots) has been successfully described within a single–particle framework. Electron–electron interactions affect the dephasing rate of the electrons at finite temperature, but otherwise electrons in the vicinity of the Fermi energy can be described as non–interacting quasi–particles. The single–particle dynamics in the dot can be affected by disorder or by the dot's boundaries. In a disordered dot, the electron moves diffusively. If the disorder is weak, the statistical fluctuations of the single–electron spectrum and wave functions can be described by random–matrix theory (RMT).[1] Similarly, in a ballistic dot with irregular boundaries, the classical dynamics are mostly chaotic and the statistical quantal fluctuations also follow RMT. In such diffusive and/or chaotic open dots, the conductance exhibits "random" but reproducible fluctuations versus, e.g., gate voltage or magnetic field that can be successfully described by RMT.[2]

The situation changes as the coupling of the dot to the leads is reduced and the dot becomes almost isolated. The charge on the dot becomes quantized, the conductance as a function of gate voltage displays sharp peaks (the Coulomb blockade resonances), and the Coulomb interaction between electrons becomes important.[2] In this Coulomb blockade regime, the simplest model for a quantum dot is the constant interaction (CI) model. The interaction is modeled by the classical charging energy of a system with capacitance C. For a fixed number of electrons n on the dot, the interaction of this model is constant, and the model essentially reduces to a single–particle model. While certain statistical properties of the conductance peak heights can be described within the CI plus RMT model,[3,4] other observables, most notably the distribution of the distance between successive conductance peaks (a distance known as the peak spacing), deviate significantly from the predictions of the CI plus RMT model.[5,6,7,8] These deviations have been understood, at least qualitatively, to follow from residual interaction effects beyond the charging energy.[5,9,10] Such residual interaction effects are at the center of the present investigation.

In a weakly diffusive and/or chaotic dot, the "randomness" of the single–particle eigenfunctions induces randomness of the interaction matrix elements. The statistical fluctuations of these interaction matrix elements (evaluated in the non–interacting basis) were calculated for a dot with a large Thouless conductance g[9,11] and were found to be suppressed. In the limit $g \to \infty$, only a few interaction terms survive, leading to the so–called universal Hamiltonian.[12,13] For spinless electrons, the interaction part of the universal Hamiltonian is composed of just the charging energy term. This shows that the CI

model is appropriate for spinless electrons and in the limit $g \to \infty$. When the electron spin is taken into account, there is also an exchange interaction term, and, in the absence of a time–reversal–symmetry breaking magnetic field, a Cooper–channel–like term. The exchange interaction term was found to have important effects on the finite–temperature peak spacing distribution.[14,15] For finite g, further interaction terms exist and can be calculated within a systematic expansion of the residual interaction in inverse powers of g. Using a two–body effective screened interaction in the limit of a small gas constant r_s, one can show that for a diffusive dot the average and the standard deviation of these residual interaction terms are at least of the order Δ/g, where Δ is the single–particle mean level spacing, while for a chaotic dot the standard deviation of the residual interaction terms is of the order $\Delta\sqrt{\ln g}/g$.[16,17] For finite values of g, such terms affect the ground–state energy of the dot and various observables. In particular, the position of the conductance peak height at low temperatures is determined by the change of the ground–state energy upon the addition of an electron to the dot (addition energy). Thus, finite–g–corrections to the universal Hamiltonian affect the peak–spacing distribution.[16,17]

Most studies of interaction effects have been limited to specific models of a dot. These models include an Anderson model for a diffusive dot or a billiard model for a ballistic chaotic dot, plus Coulomb or Hubbard–like (short–range) interactions. For a small number of electrons, exact numerical solutions are possible.[5,10] For a larger number of electrons, such models have been studied in the Hartree–Fock (HF) approximation[18,19,20] and in a density functional approach.[21,22,23] These models contributed significantly to our understanding of interaction effects in almost isolated dots, but they also contain non–generic features.

Our approach to interaction effects in diffusive and/or chaotic, almost isolated quantum dots aims at a generic understanding of interaction effects beyond the $g \to \infty$ limit. Our starting point is a Hamiltonian consisting of a one–body and a two–body part. The one–body part describes chaos and/or disorder and is, within an energy interval of width $\approx g\Delta$, described by the appropriate random–matrix ensemble, i.e., the orthogonal ensemble for conserved time–reversal symmetry and the unitary ensemble for broken time–reversal symmetry. The two–body part is given by the Coulomb interaction. However, the randomness of the single–particle wave functions induces a randomness of the two–body interaction matrix elements when the latter are written in terms of the eigenfunctions of the random one–body part of the Hamiltonian. This results in a generic ensemble of the two–body interaction that we derive and use in our studies.

The paper consists of two parts. In the first part, we derive the statistical properties of the two–body matrix elements (the "induced two–body ensemble"). We find that these properties are determined both by the underlying space–time symmetries of the system and by features of the two–body interaction. We classify the possible forms of the first two cumulants of the interaction matrix elements. This is accomplished by writing these cumulants in a covariant form, ensuring invariance under a change of the single–particle basis. The first moments (average values) reproduce the universal Hamiltonian in the limit $g \to \infty$. The second cumulants are characterized by a constant u^2 ($u^2 \propto \Delta^2/g^2$ for a diffusive dot and $u^2 \propto \Delta^2 \ln g/g^2$ for a chaotic dot). The invariance classes of the second cumulants are determined by the symmetry properties of the interaction matrix elements under permutations of the single–particle orbitals. These symmetries are different for, e.g., a contact interaction or a short– but finite–range interaction. We note that the two–body part of one class of the ensembles which we construct, coincides with the two–body embedded Gaussian ensembles.[24] These ensembles were introduced in the nuclear shell model to study the validity of RMT for the statistical description of nuclear spectra.[25,26] The spectral properties of these embedded ensembles were recently analyzed using an eigenvector expansion of the second moments.[27,28] Combined with a random–matrix one–body part, such a two–body ensemble was used to study interaction effects[29,30] and ground-state magnetization[31] in quantum dots with a small number of electrons. The spin structure of a system with a spin–conserving random interaction was studied in Ref. 32.

In the presence of spin degrees of freedom, one needs to use non–antisymmetrized two–body matrix elements, and our classification of the second cumulants is generally done for such elements. The spinless case requires only antisymmetrized matrix elements. Their second cumulants are obtained directly from the cumulants of the non–antisymmetrized elements. The two–body ensembles that correspond to a contact interaction exist only in the presence of spin.

In the second part of the paper, we use the Hartree–Fock (HF) approximation to work out interaction effects for some of the ensembles introduced in the first part. It is difficult to study the properties of ensembles involving a two–body interaction. Exact numerical solutions can be obtained only for dots with a small number of electrons. For a larger number of electrons, it is necessary to make approximations. The HF approximation serves this purpose. It has the advantage of being based on a single–particle picture (optimized to take into account interaction effects), and one can still use concepts familiar from the independent–particle approach. While the HF approximation has been studied in the context of specific models for an interacting dot,[18,19,20] the present work is free of any model–dependent effects and constitutes a generic statistical HF approach.

Our HF studies are limited to spinless electrons. We investigate, in particular, the statistical properties of the interaction matrix elements in the basis of HF single–particle eigenfunctions, and of the HF single–particle eigenvalues and eigenfunctions. The interest in such work

derives, among others, from generic studies of quantum dots with a large number of electrons. These often use a HF single–particle basis (rather than a basis defined in terms of non–interacting electrons).[16] It is then often assumed that the statistical properties of the matrix elements in the HF basis are similar to those of the non–interacting basis.[9] Our work permits us to test such assumptions, whereas previous studies (done in the framework of specific models of a dot with interactions) have focused on the spectral statistics of the HF levels only. We find that, in the limit of small interaction strength u, the average interaction matrix elements in the HF basis acquire a u^2 correction (this explains the increase of the average HF gap with u), while the second cumulants remain very close to their input values. As for the spectral statistics, our generic studies confirm the conclusions of previous studies. The nearest–neighbor spacings of filled and empty HF levels follow the Wigner distribution of RMT, while the distribution of the HF gap deviates from this distribution. An open problem has been whether correlations of filled and empty levels follow or deviate from RMT. Our studies of an appropriate spacing correlator indicate that the gap weakens the correlations between spacings on its opposite sides. On the other hand, this spacing correlator is found to follow RMT within the filled or empty levels alone, adding further support to the conjecture that the filled and empty levels separately satisfy RMT statistics. We also show that the HF ensemble satisfies orthogonal (unitary) invariance, and therefore its wave function statistics is that of RMT.

We use the statistical HF approach to study the statistics of observables, and in particular of the peak–spacing and peak–height distributions. The results can be easily interpreted in Koopmans' limit,[33] which assumes that the HF wave functions remain unchanged upon the addition (or removal) of an electron. Koopmans' limit has been investigated in previous HF studies,[18,19,20] but the present approach again has the advantage of being generic. It allows us to define the limitations of Koopmans' approach, and to go beyond that limit. In particular, we find that the peak–spacing distribution can be described as a convolution of a Wigner distribution (with an appropriate mean level spacing) and a Gaussian whose width is approximately the standard deviation of a diagonal interaction matrix element. On the other hand, we find that the peak–height distribution is not affected by the residual interaction.

The outline of this paper is as follows: In Section II, we discuss the induced two–body ensembles. We classify the possible ensembles for the orthogonal and unitary symmetries in Sections II B 1 and II B 2, respectively, both in the presence and absence of the spin degrees of freedom. The possible ensembles are related to different types of two–body interactions, as characterized by the symmetries of their matrix elements under permutations of the orbitals. In Section III A we discuss the HF approach to disordered (or chaotic) systems in the framework of the many–body ensembles. A perturbative approach that provides a closed expression for the average HF matrix elements for a fixed single–particle spectrum is described in Section III B. Numerical studies of both the first and second moments of the interaction matrix elements in the HF basis are presented in Section III C. The statistics of the HF single–particle energies including filled levels, empty levels and the gap are studied in Section III D, while the statistics of the HF wave function components are studied in Section III E. Finally in Section IV we discuss the addition of electrons in the HF approach to disordered systems, and in particular the peak–spacing and peak–height distributions.

II. DISORDERED SYSTEMS WITH INTERACTIONS

We consider a disordered system of interacting electrons, e.g., a diffusive quantum dot. For simplicity, we first discuss the case of spinless electrons. The spin degrees of freedom are introduced later in this Section. For a given realization of disorder, we describe the system by a Hamiltonian with a one–body part and a two–body interaction,

$$H = \sum_{i,j} h_{ij}^{(0)} a_i^\dagger a_j + \frac{1}{2} \sum_{ijkl} v_{ij;kl} a_i^\dagger a_j^\dagger a_l a_k \ . \qquad (1)$$

The m orthonormal single–particle states $|i\rangle = a_i^\dagger |-\rangle$ $(i = 1, \ldots, m)$ with $|-\rangle$ the vacuum state, form a fixed basis with $m \gg 1$. The one–body part $h_{ij}^{(0)}$ of H stands for kinetic energy plus disorder potential, while $v_{ij;kl}$ represents the (screened) Coulomb interaction. The $v_{ij;kl} \equiv \langle ij|v|kl\rangle$ are non–antisymmetrized matrix elements of the two–body interaction ($|ij\rangle$ is a product state of particle 1 in state $|i\rangle$ and particle 2 in state $|j\rangle$). For spinless fermions, we can rewrite the interaction in terms of antisymmetrized matrix elements $v_{ij;kl}^A \equiv v_{ij;kl} - v_{ij;lk}$ as

$$H = \sum_{i,j} h_{ij}^{(0)} a_i^\dagger a_j + \frac{1}{4} \sum_{ijkl} v_{ij;kl}^A a_i^\dagger a_j^\dagger a_l a_k \ . \qquad (2)$$

Disorder is taken into account by postulating that $h_{ij}^{(0)}$ is random. The way this randomness is modeled turns out to be rather immaterial. Indeed, we recall that for weak disorder and in the long–wavelength limit, all models for non–interacting disordered systems yield the same supersymmetric field theory, the non–linear supersymmetric sigma model.[34] This field theory contains one essential parameter, the dimensionless Thouless conductance g. We will work out properties of the system described by the Hamiltonian of Eq. (2) in terms of an expansion in inverse powers of g. We will carry the expansion up to and including terms of order $1/g^2$.

The non–linear sigma model shows that to zeroth order in $1/g$, $h_{ij}^{(0)}$ is equivalent to one of the canonical ensembles of RMT, the Gaussian orthogonal (GOE), unitary (GUE)

or symplectic (GSE) ensemble of random matrices, depending upon the symmetry of the problem.[1,34] Corrections calculated by using the expansion in inverse powers of g yield deviations from predictions of RMT but do not violate the fundamental symmetries of the problem (invariance under orthogonal, unitary or symplectic transformations of the basis of single–particle states). Indeed, the derivation of the non–linear sigma model is based upon these symmetries, which are thus deeply embedded in the model and are valid beyond canonical RMT. This fact will be important as we will heavily rely on these symmetries to determine the effective form of the Hamiltonian H. We will focus on the cases of orthogonal and unitary symmetry and will not consider symplectic ensembles in the sequel.

The randomness of $h^{(0)}_{ij}$ induces a degree of randomness into the two–body matrix elements $v_{ij;kl}$. To see this we recall that every observable $\mathcal{O}$ is defined as an average over the ensemble $h^{(0)}_{ij}$. Because of the invariance of that ensemble under orthogonal (or unitary or symplectic) transformations of the single–particle basis, $\mathcal{O}$ must likewise be invariant under all such transformations. Therefore, $\mathcal{O}$ can depend on the two–body interaction $v_{ij;kl}$ only through invariants constructed from the matrix elements $v_{ij;kl}$. Other properties of the Coulomb interaction that are not encapsulated in the invariants are not relevant. On a formal level, this fact allows us to define equivalence classes of two–body interactions. Members of the same class share the same set of invariants although the interactions may differ in other properties. All two–body interactions which belong to the same class as the Coulomb interaction will give rise to identical average properties of the ensemble (1). These members may be said to form an induced ensemble of two–body interactions. The word "induced" indicates that the ensemble owes its existence to the randomness of the one–body part $h^{(0)}_{ij}$. Thus, we deal effectively with an induced two–body random ensemble although the Coulomb interaction *per se* is fixed and not random at all. We aim at reformulating the ensemble of Hamiltonians H in Eq. (1) in such a way that only the relevant features (i.e., the invariants) of $v_{ij;kl}$ are kept. In doing so, we do not follow strictly the line of argument just given because we perform separately the averages over the eigenfunctions and eigenvalues of $h^{(0)}_{ij}$. The induced two–body ensemble will result from the average over the eigenfunctions.

We accordingly transform H in Eq. (2) to the basis $|\alpha\rangle$ of single–particle eigenstates of $h^{(0)}$. This yields

$$H = \sum_{\alpha} \epsilon_\alpha a^\dagger_\alpha a_\alpha + \frac{1}{4} \sum_{\alpha\beta\gamma\delta} v^A_{\alpha\beta;\gamma\delta} a^\dagger_\alpha a^\dagger_\beta a_\delta a_\gamma \ . \qquad (3)$$

In an interval of length $\sim g\Delta$ (where Δ is the average single–particle level spacing), the eigenvalues ϵ_α obey canonical random–matrix statistics. Because of the randomness of the single–particle eigenfunctions, the elements $v^A_{\alpha\beta;\gamma\delta}$ are also random. Moreover, the ϵ_α's are uncorrelated with the eigenfunctions and, thus, with the $v_{\alpha\beta;\gamma\delta}$'s. This last property holds strictly if $h^{(0)}$ stands for the GOE or GUE, i.e., in the limit $g \to \infty$. For a diffusive system, it holds up to and including terms of order $1/g^2$.

The number of single–particle levels α is usually chosen to be finite. Thus, the interaction in Eq. (3) is generally an effective interaction, e.g., a screened Coulomb interaction. Such an effective interaction was, for example, derived in Refs. 9,13 within an interval of $\sim g$ levels around the Fermi energy of the dot. The authors used the random–phase approximation (RPA) in the limit where the gas constant $r_s \ll 1$. The effective interaction is then given by the unscreened zero–momentum Fourier component of the Coulomb interaction plus a short–range screened Coulomb interaction (whose exact form depends on the dimensionality and geometry of the system). In general, for a finite system this effective interaction also includes surface charge terms.[9] These can be eliminated by assuming, for instance, periodic boundary conditions and will not be taken into account in the sequel.

If the spin of the electrons is taken into account, the Hamiltonian (1) is replaced by

$$H = \sum_{i,j;\sigma} h^{(0)}_{ij} a^\dagger_{i\sigma} a_{j\sigma} + \frac{1}{2} \sum_{\substack{ijkl \\ \sigma\sigma'}} v_{ij;kl} a^\dagger_{i\sigma} a^\dagger_{j\sigma'} a_{l\sigma'} a_{k\sigma} \ , \qquad (4)$$

where $\sigma = \pm$ describes a spin up/down electron and $|i\rangle$ denotes an orbital state. The one–body Hamiltonian $h^{(0)}$ is spin–independent (i.e., there is no spin–orbit coupling). The interaction matrix elements are also assumed to be spin–independent as is the case for the Coulomb interaction.

In analogy to the transformation leading from Eq. (1) to Eq. (3), the ensemble (4) can be written in terms of the orbital eigenfunctions $|\alpha\rangle$ of the one–body Hamiltonian $h^{(0)}$. Since the transformation from the basis of states $|i\rangle$ to that of the states $|\alpha\rangle$ does not involve the spin degree of freedom, the single–particle energies ϵ_α are spin–degenerate, and the interaction matrix elements remain spin–independent. Thus, when the spin is included, Eq. (3) is replaced by

$$H = \sum_{\alpha\sigma} \epsilon_\alpha a^\dagger_{\alpha\sigma} a_{\alpha\sigma} + \frac{1}{2} \sum_{\substack{\alpha\beta\gamma\delta \\ \sigma\sigma'}} v_{\alpha\beta;\gamma\delta} a^\dagger_{\alpha\sigma} a^\dagger_{\beta\sigma'} a_{\gamma\sigma'} a_{\delta\sigma} \ . \qquad (5)$$

In contrast to the spinless case where H could be expressed in terms of the antisymmetrized matrix elements v^A, Eq. (5) contains the full non–antisymmetrized interaction matrix elements.

We now work out the first and second moments of $v_{\alpha\beta;\gamma\delta}$ by averaging over the eigenfunctions $|\alpha\rangle$.

A. Mean Values

We first calculate the mean value $\bar{v}_{\alpha\beta;\gamma\delta}$ of the two–body matrix elements, invoking orthogonal or unitary

invariance. In the orthogonal case there are three invariants: $\delta_{\alpha\gamma}\delta_{\beta\delta}$, $\delta_{\alpha\delta}\delta_{\beta\gamma}$, and $\delta_{\alpha\beta}\delta_{\gamma\delta}$. In the unitary case, only the first two invariants exist. We consider first the case of antisymmetrized matrix elements and include spin below. For the antisymmetrized element $v^A_{\alpha\beta;\gamma\delta} \equiv v_{\alpha\beta;\gamma\delta} - v_{\alpha\beta;\delta\gamma}$, the first two invariants combine to $\delta_{\alpha\gamma}\delta_{\beta\delta} - \delta_{\alpha\delta}\delta_{\beta\gamma}$, while the third one gives no contribution. We conclude (for both the orthogonal and unitary symmetries) that

$$\bar{v}^A_{\alpha\beta;\gamma\delta} = v_0(\delta_{\alpha\gamma}\delta_{\beta\delta} - \delta_{\alpha\delta}\delta_{\beta\gamma}) \ . \tag{6}$$

The average interaction in (3) is then given by

$$\bar{v} = \frac{1}{2}v_0(\hat{n}^2 - \hat{n}) \ , \tag{7}$$

where $\hat{n}$ is the particle–number operator. For a fixed number n of fermions, the average interaction is simply a constant $v_0(n^2 - n)/2$. For a quantum dot, the zero–momentum Fourier component of the Coulomb interaction is unscreened and its contribution to v_0 is the charging energy e^2/C where C is the dot's capacitance. The contribution of the screened short–range Coulomb interaction can be estimated using the diagrammatic expansion and is of order Δ. For finite g, there are corrections of order $1/g$.

For the case with spin, all three (two) orthogonal (unitary) invariants now contribute to the value of the average interaction,

$$\bar{v}_{\alpha\beta;\gamma\delta} = v_0\delta_{\alpha\gamma}\delta_{\beta\delta} + J_s\delta_{\alpha\delta}\delta_{\beta\gamma} + J_c\delta_{\alpha\delta}\delta_{\beta\gamma} \ . \tag{8}$$

Here v_0, J_s and J_c are constants and the last term on the r.h.s. is absent for the unitary case. Using Eq. (8) in Eq. (5) we obtain an average interaction of the form

$$\bar{v} = \frac{1}{2}(v_0 - J_s/2)\hat{n}^2 - (v_0/2 - J_s)\hat{n} - J_s\hat{\mathbf{S}}^2 + J_c\hat{T}^\dagger\hat{T} \ . \tag{9}$$

In Eq. (9), $\hat{\mathbf{S}} = \frac{1}{2}\sum_\alpha \sum_{\sigma\sigma'} a^\dagger_{\alpha\sigma}\hat{\sigma}_{\sigma\sigma'}a_{\alpha\sigma'}$ is the total spin operator of the dot, where $\hat{\sigma}$ is the vector of the three 2×2 Pauli matrices. The operator $\hat{T}^\dagger = \sum_\alpha a^\dagger_{\alpha+}a^\dagger_{\alpha-}$ creates coherent pairs of spin up–down electrons. Adding the average interaction (9) to the one–body part of Eq. (5) and taking the limit $g \to \infty$, we obtain the universal Hamiltonian of the quantum dot, with $v_0 = \bar{v}_{\alpha\beta;\alpha\beta}$, $J_s = \bar{v}_{\alpha\beta;\beta\alpha}$, and $J_c = \bar{v}_{\alpha\alpha;\beta\beta}$ the direct, exchange and the Cooper channel interaction strengths, respectively.[12,13] We note, however, that Eq. (9) is valid beyond this limit. For finite values of g, corrections to the various constants can be obtained by the diagrammatic expansion in $1/g$. Unlike the charging energy term (which for a fixed number of electrons is simply a constant), the exchange and Cooper channel interactions are represented by non–trivial operators.

B. Second Moments

The second moments of the interaction matrix elements depend upon the symmetry of the ensemble, and upon the generic form of the two–body interaction. It is easier to calculate first the second moments of the non–antisymmetrized matrix elements $v_{\alpha\beta;\gamma\delta}$ for the two–body ensemble in the presence of spin degrees of freedom. The spinless case is then obtained by considering the corresponding moments of the antisymmetrized matrix elements $v^A_{\alpha\beta;\gamma\delta}$.

To simplify the notation, we assume in the following that the average interaction has been separated out and put $\bar{v}_{\alpha\beta;\gamma\delta} = 0$.

1. *Orthogonal induced two–body ensembles*

In the case of orthogonal symmetry the two–body interaction matrix $v_{\alpha\beta;\gamma\delta}$ is real and symmetric, $v_{\alpha\beta;\gamma\delta} = v^*_{\alpha\beta;\gamma\delta} = v_{\gamma\delta;\alpha\beta}$. Depending on the form of the interaction, we distinguish three induced ensembles.

(i) For a schematic effective interaction that is a δ–function (i.e., contact interaction), the matrix element $v_{\alpha\beta;\gamma\delta} = V\Delta \int d\mathbf{r}\psi_\alpha(\mathbf{r})\psi_\beta(\mathbf{r})\psi_\gamma(\mathbf{r})\psi_\delta(\mathbf{r})$ (V is the volume and Δ is the single–particle mean–level spacing) is invariant under all 24 permutations of the four indices $\alpha\beta\gamma\delta$. An ensemble of two–body matrix elements that satisfies the orthogonal invariance condition and is consistent with the symmetries of $v_{\alpha\beta;\gamma\delta}$, is expected to have to leading order in $1/g$ (see below) a second moment of the form[35]

$$\overline{v_{\alpha\beta;\gamma\delta}v_{\mu\nu;\rho\sigma}} = 3u^2(\delta_{\alpha\mu}\delta_{\beta\nu}\delta_{\gamma\rho}\delta_{\delta\sigma} + \ldots) \tag{10}$$

where $\ldots$ stands for the sum of terms obtained by all 23 permutations of $\mu\nu\rho\sigma$. Non–linear sigma model calculations,[11] as well as diagrammatic calculations in weakly disordered systems using a screened Coulomb interaction, show that $u^2 \propto \Delta^2/g^2$ (see below). We have written down only invariants that arise by pairing indices appearing in different matrix elements. Invariance requirements alone would also allow terms involving Kronecker symbols like $\delta_{\alpha\beta}$ etc. However, in diffusive systems such invariant terms are at least of third order in $1/g$ and are, therefore, ignored. An analogous statement applies to all the other induced two–body ensembles listed below, both for the orthogonal and the unitary cases, and will not be repeated there.

For a diffusive dot, the quantity u^2 in Eq. (10) can be calculated in the diagrammatic approach. If the energy difference between any pair of levels from the set $\alpha\beta\gamma\delta$ is smaller than the Thouless energy $g\Delta$, Eq. (10) is found with[9,36]

$$u^2 = \int d\mathbf{r} \int d\mathbf{r}' \ \Pi^2(\mathbf{r},\mathbf{r}')/V^2 = c\frac{\Delta^2}{g^2} \ , \tag{11}$$

independently of the energy differences of the single–particle levels. Here $\Pi(\mathbf{r}_1,\mathbf{r}_2) = (V\Delta/\pi)\sum_{\mathbf{Q}\neq\mathbf{0}}\phi_{\mathbf{Q}}(\mathbf{r}_1)\phi_{\mathbf{Q}}(\mathbf{r}_2)/D\mathbf{Q}^2$ is the diffusion propagator in the finite dot, with $\phi_{\mathbf{Q}}$ the eigenfunction of the diffusion operator corresponding to the eigenvalue

$D\mathbf{Q}^2$. The proportionality constant c in Eq. (11) depends on the geometry of the dot. For a cubic dot of length L in d dimensions, $c = \frac{4}{\pi^4}\sum_{\mathbf{n}\neq 0} 1/|\mathbf{n}|^{\mathbf{4}}$ where $\mathbf{n}$ is a vector of d non–negative integers (and the dimensionless conductance g is defined by $g\Delta = 2\pi\hbar D/L^2$).[36] For a 2D circular dot of radius R, $c = 2[\sum_{l,m} x_{l,m}^{-4}]^{1/2} \approx 0.67$ where $x_{l,m}$ are the zeros of the derivative of the Bessel function of order l (and the dimensionless conductance is defined by $g\Delta = 2\pi\hbar D/R^2$).[16] In the general case where some of the energy differences between pairs of levels are greater than $g\Delta$, the coefficient c in Eq. (11) is no longer constant but depends on these energy differences.

Eq. (11) can be extended to a ballistic dot. This is done with the help of a supersymmetric sigma model, obtained through the addition of weak disorder with finite correlation length.[37] In the ballistic case[30]

$$u^2 = c'\frac{\Delta^2}{g^2}\ln(c''g)\ , \tag{12}$$

where $g = \pi(n/2)^{1/2}$ is the ballistic Thouless conductance, n is the number of electrons, and $c' = 3/4$ is a geometry–independent constant. The constant c'' depends on the geometry of the dot. For a circular ballistic dot, $c'' \approx 0.81$.

From Eq. (10), the variances of off–diagonal and diagonal matrix elements are given by ($\alpha, \beta, \gamma, \delta$ are all different)

$$\sigma^2(v_{\alpha\beta;\gamma\delta}) = 3u^2 \quad , \quad \sigma^2(v_{\alpha\beta;\alpha\beta}) = 12u^2\ ,$$
$$\sigma^2(v_{\alpha\alpha;\alpha\alpha}) \ = \ 72u^2\ . \tag{13}$$

For spinless fermions, we have $v^A_{\alpha\beta;\gamma\delta} = v_{\alpha\beta;\gamma\delta} - v_{\alpha\beta;\delta\gamma} = 0$ because of the symmetries satisfied by the v's. Therefore, there is no non–trivial ensemble of antisymmetrized matrix elements that corresponds to Eq. (10), and the ensemble (10) exists only when the spin degrees of freedom are taken into account.

(ii) For a generic two–body local symmetric interaction $v(\mathbf{r_1}, \mathbf{r_2}) = v(\mathbf{r_2}, \mathbf{r_2})$, the matrix elements satisfy the relations

$$v_{\alpha\beta;\gamma\delta} = v_{\beta\alpha;\delta\gamma} = v_{\gamma\delta;\alpha\beta} = v_{\delta\gamma;\beta\alpha} = v_{\gamma\beta;\alpha\delta} = v_{\beta\gamma;\delta\alpha} = v_{\alpha\delta;\gamma\beta} = v_{\delta\alpha;\beta\gamma}\ . \tag{14}$$

The second moment of the ensemble is expected to have the form

$$\overline{v_{\alpha\beta;\gamma\delta}v_{\mu\nu;\rho\sigma}} = u^2(\delta_{\alpha\mu}\delta_{\beta\nu}\delta_{\gamma\rho}\delta_{\delta\sigma} + \delta_{\alpha\nu}\delta_{\beta\mu}\delta_{\gamma\sigma}\delta_{\delta\rho} + \delta_{\alpha\rho}\delta_{\beta\sigma}\delta_{\gamma\mu}\delta_{\delta\nu} + \delta_{\alpha\sigma}\delta_{\beta\rho}\delta_{\gamma\nu}\delta_{\delta\mu} +$$
$$\delta_{\alpha\rho}\delta_{\beta nu}\delta_{\gamma\mu}\delta_{\delta\sigma} + \delta_{\alpha\nu}\delta_{\beta\rho}\delta_{\gamma\sigma}\delta_{\delta mu} + \delta_{\alpha\mu}\delta_{\beta\sigma}\delta_{\gamma\rho}\delta_{\delta\nu} + \delta_{\alpha\sigma}\delta_{\beta\mu}\delta_{\gamma\nu}\delta_{\delta\rho})\ , \tag{15}$$

where the eight terms correspond to the eight permutations of $\mu\nu\rho\sigma$ that leave $v_{\mu\nu\rho\sigma}$ invariant (see Eqs. (14)). The form (15) is also obtained in the diagrammatic approach to order $1/g^2$ when an RPA two–body screened interaction $v(\mathbf{r_1}, \mathbf{r_2})$ is used. In the limit $r_s \ll 1$, some of the diagrams that do contribute for a δ–function interaction, give a negligible contribution for a local finite–range interaction,[35] this leading to Eq. (15) instead of Eq. (10). The factor u^2 is still given approximately by Eq. (11), but now

$$\sigma^2(v_{\alpha\beta;\gamma\delta}) = u^2\ ,\ \ \sigma^2(v_{\alpha\beta;\alpha\beta}) = 4u^2\ ,\ \ \sigma^2(v_{\alpha\beta;\beta\alpha}) = 2u^2\ ,\ \ \sigma^2(v_{\alpha\alpha;\alpha\alpha}) = 8u^2\ . \tag{16}$$

The direct ($v_{\alpha\beta;\gamma\delta}$) and exchange ($v_{\alpha\beta;\delta\gamma}$) matrix elements are uncorrelated. The ensemble of antisymmetrized matrix elements $v^A_{\alpha\beta;\gamma\delta}$ follows from Eq. (15) using $\overline{v^A_{\alpha\beta;\gamma\delta}v^A_{\mu\nu;\rho\sigma}} = \overline{v_{\alpha\beta;\gamma\delta}v_{\mu\nu;\rho\sigma}} + \overline{v_{\alpha\beta;\delta\gamma}v_{\mu\nu;\sigma\rho}} - \overline{v_{\alpha\beta;\gamma\delta}v_{\mu\nu;\sigma\rho}} - \overline{v_{\alpha\beta;\delta\gamma}v_{\mu\nu;\rho\sigma}}$. We find

$$\begin{aligned}\overline{v^A_{\alpha\beta;\gamma\delta}v^A_{\mu\nu;\rho\sigma}} = {} & 2u^2(\delta_{\alpha\mu}\delta_{\beta\nu}\delta_{\gamma\rho}\delta_{\delta\sigma} - \delta_{\alpha\mu}\delta_{\beta\nu}\delta_{\gamma\sigma}\delta_{\delta\rho} + \delta_{\alpha\nu}\delta_{\beta\mu}\delta_{\gamma\sigma}\delta_{\delta\rho} - \delta_{\alpha\nu}\delta_{\beta\mu}\delta_{\gamma\rho}\delta_{\delta\sigma} \\ & +\delta_{\alpha\rho}\delta_{\beta\sigma}\delta_{\gamma\mu}\delta_{\delta\nu} - \delta_{\alpha\sigma}\delta_{\beta\rho}\delta_{\gamma\mu}\delta_{\delta\nu} + \delta_{\alpha\sigma}\delta_{\beta\rho}\delta_{\gamma\nu}\delta_{\delta\mu} - \delta_{\alpha\rho}\delta_{\beta\sigma}\delta_{\gamma\nu}\delta_{\delta\mu}) \\ & +u^2(\delta_{\alpha\rho}\delta_{\beta\nu}\delta_{\gamma\mu}\delta_{\delta\sigma} - \delta_{\alpha\sigma}\delta_{\beta\nu}\delta_{\gamma\mu}\delta_{\delta\rho} + \delta_{\alpha\nu}\delta_{\beta\rho}\delta_{\gamma\sigma}\delta_{\delta\mu} - \delta_{\alpha\nu}\delta_{\beta\sigma}\delta_{\gamma\rho}\delta_{\delta\mu} \\ & +\delta_{\alpha\mu}\delta_{\beta\sigma}\delta_{\gamma\rho}\delta_{\delta\nu} - \delta_{\alpha\mu}\delta_{\beta\rho}\delta_{\gamma\sigma}\delta_{\delta\nu} + \delta_{\alpha\sigma}\delta_{\beta\mu}\delta_{\gamma\nu}\delta_{\delta\rho} - \delta_{\alpha\rho}\delta_{\beta\mu}\delta_{\gamma\nu}\delta_{\delta\sigma} \\ & +\delta_{\alpha\sigma}\delta_{\beta\nu}\delta_{\gamma\rho}\delta_{\delta\mu} - \delta_{\alpha\rho}\delta_{\beta\nu}\delta_{\gamma\sigma}\delta_{\delta\mu} + \delta_{\alpha\nu}\delta_{\beta\sigma}\delta_{\gamma\mu}\delta_{\delta\rho} - \delta_{\alpha\nu}\delta_{\beta\rho}\delta_{\gamma\mu}\delta_{\delta\sigma} \\ & +\delta_{\alpha\mu}\delta_{\beta\rho}\delta_{\gamma\nu}\delta_{\delta\sigma} - \delta_{\alpha\mu}\delta_{\beta\sigma}\delta_{\gamma\nu}\delta_{\delta\rho} + \delta_{\alpha\rho}\delta_{\beta\mu}\delta_{\gamma\sigma}\delta_{\delta\nu} - \delta_{\alpha\sigma}\delta_{\beta\mu}\delta_{\gamma\rho}\delta_{\delta\nu})\ .\end{aligned} \tag{17}$$

In particular

$$\sigma^2(v^A_{\alpha\beta;\gamma\delta}) = 2u^2\ ,\ \ \sigma^2(v^A_{\alpha\beta;\alpha\beta}) = 6u^2\ . \tag{18}$$

(iii) The matrix elements of a generic non–local two–body interaction $v(\mathbf{r_1}, \mathbf{r_2}; \mathbf{r'_1}, \mathbf{r'_2}) = v(\mathbf{r_2}, \mathbf{r_1}; \mathbf{r'_2}, \mathbf{r'_1})$ (we define $v(\mathbf{r_1}, \mathbf{r_2}; \mathbf{r'_1}, \mathbf{r'_2}) \equiv \langle \mathbf{r_1}, \mathbf{r_2}|v|\mathbf{r'_1}, \mathbf{r'_2}\rangle$) satisfy

$$v_{\alpha\beta;\gamma\delta} = v_{\beta\alpha;\delta\gamma} = v_{\gamma\delta;\alpha\beta} = v_{\delta\gamma;\beta\alpha}\ . \tag{19}$$

Therefore, we expect for the ensemble average

$$\overline{v_{\alpha\beta;\gamma\delta}v_{\mu\nu;\rho\sigma}} = u^2(\delta_{\alpha\mu}\delta_{\beta\nu}\delta_{\gamma\rho}\delta_{\delta\sigma} + \delta_{\alpha\nu}\delta_{\beta\mu}\delta_{\gamma\sigma}\delta_{\delta\rho} + \delta_{\alpha\rho}\delta_{\beta\sigma}\delta_{\gamma\mu}\delta_{\delta\nu} + \delta_{\alpha\sigma}\delta_{\beta\rho}\delta_{\gamma\nu}\delta_{\delta\mu}) \ , \tag{20}$$

i.e., the two–body Gaussian orthogonal ensemble. The corresponding variances are given by

$$\sigma^2(v_{\alpha\beta;\gamma\delta}) = u^2 \ , \ \ \sigma^2(v_{\alpha\beta;\alpha\beta}) = 2u^2 \ , \ \ \sigma^2(v_{\alpha\beta;\beta\alpha}) = 2u^2 \ , \ \ \sigma^2(v_{\alpha\alpha;\alpha\alpha}) = 4u^2 \ . \tag{21}$$

For the antisymmetrized interaction matrix elements we expect accordingly

$$\begin{aligned}\overline{v^A_{\alpha\beta;\gamma\delta}v^A_{\mu\nu;\rho\sigma}} = 2u^2(&\delta_{\alpha\mu}\delta_{\beta\nu}\delta_{\gamma\rho}\delta_{\delta\sigma} - \delta_{\alpha\mu}\delta_{\beta\nu}\delta_{\gamma\sigma}\delta_{\delta\rho} + \delta_{\alpha\nu}\delta_{\beta\mu}\delta_{\gamma\sigma}\delta_{\delta\rho} - \delta_{\alpha\nu}\delta_{\beta\mu}\delta_{\gamma\rho}\delta_{\delta\sigma} \\ &+\delta_{\alpha\rho}\delta_{\beta\sigma}\delta_{\gamma\mu}\delta_{\delta\nu} - \delta_{\alpha\sigma}\delta_{\beta\rho}\delta_{\gamma\mu}\delta_{\delta\nu} + \delta_{\alpha\sigma}\delta_{\beta\rho}\delta_{\gamma\nu}\delta_{\delta\mu} - \delta_{\alpha\rho}\delta_{\beta\sigma}\delta_{\gamma\nu}\delta_{\delta\mu}) \ .\end{aligned} \tag{22}$$

In particular

$$\sigma^2(v^A_{\alpha\beta;\gamma\delta}) = 2u^2 \ , \ \ \sigma^2(v^A_{\alpha\beta;\alpha\beta}) = 4u^2 \ . \tag{23}$$

These relations should be compared with Eqs. (18). It is not clear whether there is an interaction model for which disorder averaging leads to the ensemble (22), although this ensemble seems to be generic for non–local interactions.

2. Unitary induced two–body ensembles

For the unitary symmetry the two–body interaction matrix is complex Hermitean, $v_{\alpha\beta;\gamma\delta} = v^*_{\gamma\delta;\alpha\beta}$. There are two possible two–body ensembles:
(i) The matrix elements $v_{\alpha\beta;\gamma\delta}$ satisfy the relations

$$v_{\alpha\beta;\gamma\delta} = v_{\beta\alpha;\gamma\delta} = v_{\alpha\beta;\delta\gamma} = v_{\beta\alpha;\delta\gamma} = v^*_{\gamma\delta;\alpha\beta} = v^*_{\gamma\delta;\beta\alpha} = v^*_{\delta\gamma;\alpha\beta} = v^*_{\gamma\delta;\beta\alpha} \ . \tag{24}$$

The ensemble consistent with relations (24) is

$$\overline{v^*_{\alpha\beta;\gamma\delta}v_{\mu\nu;\rho\sigma}} = 2u^2(\delta_{\alpha\mu}\delta_{\beta\nu}\delta_{\gamma\rho}\delta_{\delta\sigma} + \delta_{\alpha\nu}\delta_{\beta\mu}\delta_{\gamma\rho}\delta_{\delta\sigma} + \delta_{\alpha\mu}\delta_{\beta\nu}\delta_{\gamma\sigma}\delta_{\delta\rho} + \delta_{\alpha\nu}\delta_{\beta\mu}\delta_{\gamma\sigma}\delta_{\delta\rho}) \ . \tag{25}$$

In the disorder basis such an ensemble is realized for a δ–function interaction with u^2 given by Eq. (11). Variances of diagonal and off–diagonal elements are given by

$$\sigma^2(v_{\alpha\beta;\gamma\delta}) = 2u^2 \ , \ \ \sigma^2(v_{\alpha\beta;\alpha\beta}) = 2u^2 \ , \ \ \sigma^2(v_{\alpha\beta;\beta\alpha}) = 2u^2 \ , \ \ \sigma^2(v_{\alpha\alpha;\alpha\alpha}) = 8u^2 \ . \tag{26}$$

Relations (24) lead to $v^A_{\alpha\beta;\gamma\delta} = 0$, so there is no non–trivial ensemble of antisymmetrized matrix elements that corresponds to Eq. (25).
(ii) The matrix elements satisfy relations that are typical for a symmetric two–body interaction (local or non–local)

$$v_{\alpha\beta;\gamma\delta} = v_{\beta\alpha;\delta\gamma} = v^*_{\gamma\delta;\alpha\beta} = v^*_{\delta\gamma;\beta\alpha} \ . \tag{27}$$

A corresponding induced two–body random matrix ensemble obeys

$$\overline{v^*_{\alpha\beta;\gamma\delta}v_{\mu\nu;\rho\sigma}} = u^2(\delta_{\alpha\mu}\delta_{\beta\nu}\delta_{\gamma\rho}\delta_{\delta\sigma} + \delta_{\alpha\nu}\delta_{\beta\mu}\delta_{\gamma\sigma}\delta_{\delta\rho}) \ , \tag{28}$$

i.e., the two–body Gaussian unitary ensemble. Such an ensemble is realized in the disorder basis by an RPA two–body screened interaction in the limit $r_s \ll 1$, with u^2 given approximately by Eq. (11). The variances of the matrix elements are

$$\sigma^2(v_{\alpha\beta;\gamma\delta}) = u^2 \ , \ \ \sigma^2(v_{\alpha\beta;\alpha\beta}) = u^2 \ \ \ \sigma^2(v_{\alpha\beta;\beta\alpha}) = u^2 \ , \ \ \sigma^2(v_{\alpha\alpha;\alpha\alpha}) = 2u^2 \ . \tag{29}$$

For the antisymmetrized interaction we find

$$\overline{v^A_{\alpha\beta;\gamma\delta}v^A_{\mu\nu;\rho\sigma}} = 2u^2(\delta_{\alpha\mu}\delta_{\beta\nu}\delta_{\gamma\rho}\delta_{\delta\sigma} - \delta_{\alpha\mu}\delta_{\beta\nu}\delta_{\gamma\sigma}\delta_{\delta\rho} + \delta_{\alpha\nu}\delta_{\beta\mu}\delta_{\gamma\sigma}\delta_{\delta\rho} - \delta_{\alpha\nu}\delta_{\beta\mu}\delta_{\gamma\rho}\delta_{\delta\sigma}) \ , \tag{30}$$

and in particular

$$\sigma^2(v^A_{\alpha\beta;\gamma\delta}) = 2u^2 \ , \ \ \sigma^2(v^A_{\alpha\beta;\alpha\beta}) = 2u^2 \ . \tag{31}$$

In the orthogonal case there was a third ensemble, but in the unitary case this third ensemble coincides with the

second one because the unitary symmetry relations (27) are common to both local and non–local interactions.

We reiterate that in the spinless case, the only non–trivial induced ensembles are (ii) and (iii) in the orthogonal case (Section II B 1), and (ii) in the unitary case (Section II B 2).

C. Induced versus true two–body ensembles

To simplify the discussion, we disregard the average part of the interaction in the ensembles (3) and (5) and put $\bar{v}_{\alpha\beta;\gamma\delta} = 0$.

So far, we have calculated only the second moments of the two–body interaction. What about higher moments? Inspection of the relevant diagrams shows that all higher–order cumulants contribute terms of order $1/g^k$ with $k \geq 3$ and are, thus, negligible in the present context. This does not necessarily imply that the induced two-body random ensembles are Gaussian. (It is conceivable that the kth cumulants are systematically of order $1/g^k$. Rescaling the matrix elements by the factor g would then yield a variable which is not Gaussian). On the other hand, numerical results in weakly diffusive systems do suggest that the interaction matrix elements have Gaussian distributions.[18] This can be attributed to a central–limit theorem: each matrix element is an integral over a product of four wave functions, and each wave function is a continuous random variable.

Our results might suggest that instead of the induced random two–body ensembles studied so far, we may use true random two–body ensembles. In the latter, the matrix elements $v_{ij;kl}$ are Gaussian–distributed random variables with mean value zero and second moments given by Eqs. (10), (15), (20), (25) or (28), as the case may be. These relations apply in any single–particle basis. In contrast to the induced random two–body ensembles, the statistical properties of the true two–body random ensembles are inherent rather than induced by the randomness of the one–body part of H. Are these two sets of ensembles pairwise equivalent? Are we allowed to replace a Hamiltonian with a random one–body and a fixed two–body interaction by a generic Hamiltonian containing both a random one–body and the random two–body interaction just defined? The answer is no, even though both Hamiltonians yield the same distributions for the two–body matrix elements. This is because in the induced two–body ensembles, randomness is due to the eigenfunctions $|\alpha\rangle$ of $h^{(0)}$. Therefore, the two–body matrix elements $v_{\alpha\beta;\gamma\delta}$ are correlated with all other expressions that depend on the $|\alpha\rangle$'s while the matrix elements of the true two–body random ensemble are independent random variables that are not correlated with other parts of the Hamiltonian. Whenever an observable contains in addition to the $v_{\alpha\beta;\gamma\delta}$'s other expressions which depend upon the $|\alpha\rangle$'s, the ensemble averages of this observable taken over the induced two–body ensemble and over the fully random two–body ensemble, will differ. However, in the numerical studies of the statistics of HF matrix elements reported below, such correlated terms do not occur, and we use the fully random two–body ensemble.

III. THE HARTREE-FOCK APPROACH TO DISORDERED SYSTEMS: FIXED NUMBER OF ELECTRONS

The theoretical treatment of a disordered system with interactions poses severe difficulties. This is why we use the HF approximation. We express observables in terms of the HF single–particle eigenvalues and eigenfunctions. We determine the latter by using the HF approximation for every realization of disorder, i.e., for every realization of a single–particle random–matrix spectrum ϵ_α and random interaction matrix elements $v_{\alpha\beta;\gamma\delta}$ in Eq. (3). This generates an ensemble of HF eigenvalues and HF eigenfunctions. We use the ensemble to calculate average values of observables as well as fluctuation properties (e.g., variances and/or distributions). In particular, we are interested in the statistical properties of the interaction matrix elements in the HF basis, and of the single–particle HF energies and wave functions.

All our calculations are done for spinless electrons. Therefore, we use the antisymmetrized matrix elements defined in the previous Section. We disregard the average matrix elements which (for a fixed number of electrons) would add only a constant to the Hamiltonian. To simplify the notation we omit the superscript A. It goes without saying that inclusion of spin degrees of freedom would be highly desirable but would obviously complicate the calculations considerably. The present paper is, thus, an exploratory study into the use of the HF approximation for a disordered system with interactions. Similar studies were previously carried out in the context of specific models, using the Coulomb interaction or a Hubbard–like short–range interaction,[18,19,20] while our work is based on the generic many–body random ensembles introduced in Section II.

In Section III A, we discuss the HF approximation in the context of the induced many–body ensembles. Sections III B and III C are devoted to the study of the statistical properties of the interaction matrix elements in the self–consistent HF basis. In particular, in Section III B we derive perturbative analytic expressions for the first two moments of the HF interaction matrix elements (assuming small u and a fixed single–particle spectrum), while in Section III C we study numerically the statistical properties of the HF interaction matrix elements. Finally, in Sections III D and III E we study the statistical properties of the HF single–particle spectrum and wave functions.

A. Hartree-Fock approximation for an interacting disordered system

In the eigenbasis of $h^{(0)}$, the single–particle HF Hamiltonian for n electrons is given by

$$h_{\alpha\gamma} = \epsilon_\alpha \delta_{\alpha\gamma} + \sum_{\beta\delta} v_{\alpha\beta;\gamma\delta}\rho_{\delta\beta} \ , \tag{32}$$

where ρ is the density matrix

$$\rho_{\delta\beta} = \sum_{l=1}^{n} \psi_l^*(\delta)\psi_l(\beta) \ . \tag{33}$$

Here $\psi_l = \sum_\alpha \psi_l(\alpha)|\alpha\rangle$ are the lowest n HF eigenstates. The latter satisfy

$$\sum_\gamma h_{\alpha\gamma}\psi_l(\gamma) = \epsilon_l^{(n)}\psi_l(\alpha) \quad \text{(for each } \alpha) \tag{34}$$

where $\epsilon_l^{(n)}$ are the single–particle HF energies for n electrons (for $n = 1$ there are no interactions and $\epsilon_l^{(1)} = \epsilon_l$). We note that the single–particle HF Hamiltonian $h_{\alpha\gamma}$ depends on the number of electrons n, but for simplicity of notation we do not indicate this dependence explicitly.

The HF equations (34) are self–consistent since the HF Hamiltonian itself is determined in terms of its n lowest eigenstates ψ_l [see Eqs. (32) and (33)]. The HF equations are solved by iteration. Starting from a particular realization of ϵ_α and $v_{\alpha\beta;\gamma\delta}$, we calculate the zeroth approximation h_0 to the HF Hamiltonian, using Eq. (32) and the density matrix $\rho^{(0)}$ given by Eq. (33), with $\psi_l^{(0)}(\beta) = \delta_{l\beta}$ (i.e., the eigenstates of $h^{(0)}$). Diagonalization of h_0 yields a new set of single–particle eigenvalues $\epsilon_{1;\sigma}$ and wave functions $\psi_\sigma^{(1)}(\alpha)$. The latter are used to construct the density matrix $\rho^{(1)}$ from Eq. (33). All this yields the one–body Hamiltonian

$$h_{1;\sigma\tau} = \epsilon_{1;\sigma}\delta_{\sigma\tau} + \sum_{\mu\nu} v_{\sigma\mu;\tau\nu}\rho_{\nu\mu}^{(1)} \ . \tag{35}$$

Diagonalizing h_1 we find its eigenvalues $\epsilon_{2;\sigma}$ and eigenstates $\psi_\sigma^{(2)}$. The latter are used in turn to construct a density matrix $\rho^{(2)}$, etc. In general, $\rho^{(2)} \neq \rho^{(1)}$ and likewise for the eigenvalues, and the iteration continues until the procedure converges to a self–consistent solution for ψ_l and $\epsilon_l^{(n)}$. To ensure convergence, it is often necessary to replace, e.g., $\rho^{(2)}$ by $\tilde{\rho}^{(2)} = (1-\lambda)\rho^{(1)} + \lambda\rho^{(2)}$, where λ $(0 < \lambda \leq 1)$ is a suitably chosen parameter.

We define the HF basis as that basis in which the HF Hamiltonian is diagonal, $h_{\sigma\tau} = \epsilon_\sigma^{(n)}\delta_{\sigma\tau}$ and $\rho_{\sigma\tau} = \delta_{\sigma\tau}\Theta(n-\sigma)$ where $\Theta(x) = 1$ for $x \geq 0$ and $\Theta(x) = 0$ for $x < 0$. The HF eigenstates σ are arranged in ascending order of the HF single–particle energies $\epsilon_\sigma^{(n)}$. The latter can be written as

$$\epsilon_\sigma^{(n)} = h_{\sigma\sigma}^{(0)} + \sum_{\tau=1}^{n} v_{\sigma\tau;\sigma\tau} \ , \tag{36}$$

where $h_{\sigma\sigma}^{(0)} = \sum_\alpha \epsilon_\alpha |\psi_\sigma(\alpha)|^2$ is a diagonal matrix element of the single–particle Hamiltonian $h^{(0)}$ in the HF basis σ. We emphasize that in general, $h_{\sigma\sigma}^{(0)} \neq \epsilon_\sigma$.

B. Moments of the Hartree–Fock matrix elements: perturbative approach

In Section III C below, we report on numerical HF calculations. The calculations are done for each realization of the many–particle ensemble (3), and statistics are collected from different realizations. This is done for either a fixed single–particle spectrum (where only the single–particle eigenfunctions are varied) or for a random single–particle spectrum (where both the single–particle energies and wave functions are varied). In either case, the resulting distribution of the two–body matrix elements in the HF basis turns out to be Gaussian. We compare the numerical results for n fermions with theoretical predictions based upon perturbation theory. To this end, we compute in the present Section the first and second moments of the two–body HF matrix elements perturbatively in leading order in u^2 for a *fixed* single–particle spectrum. We do so by using the statistics of the true (rather than of the induced) two–body ensembles introduced in Section II. This is legitimate because we average expressions that contain only the two–body matrix elements (and not other terms depending upon the eigenfunctions $|\alpha\rangle$ of $h^{(0)}$, see Section II C). We confine ourselves to the case of orthogonal symmetry. We are particularly interested in the diagonal matrix elements.

1. Perturbation expansion

We recall Eqs. (32), (33) and (34). To first order in v, the HF Hamiltonian is obtained by substituting in Eq. (32) the zeroth order expression for the one–body density matrix given by $\rho_{\delta\beta}^{(0)} = \delta_{\delta\beta}\Theta(n-\beta)$. (We assume that the eigenvalues ϵ_α are arranged in ascending order). Thus,

$$h_{0;\alpha\gamma} = \epsilon_\alpha\delta_{\alpha\gamma} + \sum_{\delta=1}^{n} v_{\alpha\delta;\gamma\delta}^{(0)} \ , \tag{37}$$

where $v^{(0)}$ denotes a matrix element in the basis of eigenstates $|\alpha\rangle$ of $h^{(0)}$.

Regarding $\sum_{\delta=1}^{n} v_{\alpha\delta;\gamma\delta}^{(0)}$ as a perturbation to the Hamiltonian $h^{(0)}$, we see that a HF eigenstate is (to first order in $v^{(0)}$) given by

$$|\alpha\rangle_{\rm HF} = |\alpha\rangle + \sum_{\mu\neq\alpha} r_{\alpha\mu}^{(1)}|\mu\rangle \ , \tag{38}$$

where

$$r_{\alpha\mu}^{(1)} = \frac{1}{\epsilon_\alpha - \epsilon_\mu}\sum_\delta \Theta(n-\delta)v_{\mu\delta;\alpha\delta}^{(0)} \ . \tag{39}$$

Using Eq. (38), we find that to second order in $v^{(0)}$ the matrix element $v_{\alpha\delta;\gamma\delta}$ in the HF basis is given by

$$v_{\alpha\beta;\gamma\delta} = v^{(0)}_{\alpha\beta;\gamma\delta} + \sum_{\mu\neq\alpha} r^{(1)}_{\alpha\mu} v^{(0)}_{\mu\beta;\gamma\delta} + \sum_{\mu\neq\beta} r^{(1)}_{\beta\mu} v^{(0)}_{\alpha\mu;\gamma\delta} + \sum_{\mu\neq\gamma} r^{(1)}_{\gamma\mu} v^{(0)}_{\alpha\beta;\mu\delta} + \sum_{\mu\neq\delta} r^{(1)}_{\delta\mu} v^{(0)}_{\alpha\beta;\gamma\mu} \; . \tag{40}$$

To calculate the variance of a HF matrix element $v_{\alpha\beta;\gamma\delta}$ to fourth order in u, we need to expand $v_{\alpha\beta;\gamma\delta}$ up to third order in $v^{(0)}$. This requires an expansion of the HF state to second order in $v^{(0)}$,

$$|\alpha\rangle_{\rm HF} = \left(1 - \frac{1}{2}\sum_{\mu\neq\alpha}(r^{(1)}_{\alpha\mu})^2\right)|\alpha\rangle + \sum_{\mu\neq\alpha} r^{(1)}_{\alpha\mu}|\mu\rangle + \sum_{\mu\neq\alpha} r^{(2)}_{\alpha\mu}|\mu\rangle \; , \tag{41}$$

where $r^{(1)}$ and $r^{(2)}$ are of first and second order in $v^{(0)}$, respectively. The matrix element is then expanded as

$$\begin{aligned} v_{\alpha\beta;\gamma\delta} \;=\; & \left(1 - \frac{1}{2}\sum_{\mu\neq\alpha}(r^{(1)}_{\alpha\mu})^2 - \frac{1}{2}\sum_{\mu\neq\beta}(r^{(1)}_{\beta\mu})^2 - \frac{1}{2}\sum_{\mu\neq\gamma}(r^{(1)}_{\gamma\mu})^2 - \frac{1}{2}\sum_{\mu\neq\delta}(r^{(1)}_{\delta\mu})^2\right) v^{(0)}_{\alpha\beta;\gamma\delta} \\ & + \left[\sum_{\mu\neq\alpha}(r^{(1)}_{\alpha\mu} + r^{(2)}_{\alpha\mu}) v^{(0)}_{\mu\beta;\gamma\delta} + \ldots\right] + \left[\sum_{\mu\neq\alpha;\nu\neq\beta} r^{(1)}_{\alpha\mu} r^{(1)}_{\beta\nu} v^{(0)}_{\mu\nu;\gamma\delta} + \ldots\right] \; , \end{aligned} \tag{42}$$

where $r^{(1)}_{\alpha\mu}$ is given by Eq. (39). To find $r^{(2)}_{\alpha\mu}$ we have to expand the HF Hamiltonian to second order in $v^{(0)}$ and use the perturbation expansion for the single–particle wave functions up to second order. The HF Hamiltonian $h^{(2)}$ is found to second order in $v^{(0)}$ by expanding the one–body density to first order in $v^{(0)}$,

$$\rho_{\delta\beta} = \sum_{l=l}^{n} \psi_l - \delta\psi_l(\beta) = \delta_{\delta\beta}\Theta(n-\beta) + [r^{(1)}_{\delta\beta}\Theta(n-\delta) + r^{(1)}_{\beta\delta}\Theta(n-\beta)](1-\delta_{\beta\delta}) \; . \tag{43}$$

Substituting this into Eq. (32) we find

$$\begin{aligned} h^{(2)}_{\alpha\gamma} \;&=\; \epsilon_\alpha\delta_{\alpha\gamma} + \sum_\delta v^{(0)}_{\alpha\delta;\gamma\delta}\Theta(n-\delta) + \sum_{\beta\delta} v^{(0)}_{\alpha\beta;\gamma\delta}[r^{(1)}_{\delta\beta}\Theta(n-\delta) + r^{(1)}_{\beta\delta}\Theta(n-\beta)](1-\delta_{\beta\delta}) \\ &=\; \epsilon_\alpha\delta_{\alpha\gamma} + \sum_\delta v^{(0)}_{\alpha\delta;\gamma\delta}\Theta(n-\delta) + \sum_{\beta,\delta}(v^{(0)}_{\alpha\beta;\gamma\delta} + v^{(0)}_{\gamma\beta;\alpha\delta}) r^{(1)}_{\delta\beta}\Theta(n-\delta)\Theta(\beta-n-1) \; . \end{aligned} \tag{44}$$

For $r^{(2)}$ this yields

$$r^{(2)}_{\alpha\mu} = \frac{1}{\epsilon_\alpha - \epsilon_\mu}\sum_\delta \Theta(n-\delta)\left[\sum_\eta (v^{(0)}_{\alpha\eta;\mu\delta} + v^{(0)}_{\mu\eta;\alpha\delta}) r^{(1)}_{\delta\eta}\Theta(\eta-n-1) + \sum_{\nu\neq\alpha} v^{(0)}_{\mu\delta;\nu\delta} r^{(1)}_{\alpha\nu} - v^{(0)}_{\alpha\delta;\alpha\delta} r^{(1)}_{\alpha\mu}\right] \; . \tag{45}$$

For the diagonal matrix elements this yields

$$\begin{aligned} v_{\alpha\beta;\alpha\beta} \;=\; & \left(1 - \sum_{\mu\neq\alpha}(r^{(1)}_{\alpha\mu})^2 - \sum_{\mu\neq\beta}(r^{(1)}_{\beta\mu})^2\right) v^{(0)}_{\alpha\beta;\alpha\beta} + \left[2\sum_{\mu\neq\alpha}(r^{(1)}_{\alpha\mu} + r^{(2)}_{\alpha\mu}) v^{(0)}_{\mu\beta;\alpha\beta} + \alpha\leftrightarrow\beta\right] \\ & + 2\sum_{\mu\neq\alpha;\nu\neq\beta} r^{(1)}_{\alpha\mu} r^{(1)}_{\beta\nu}\left(v^{(0)}_{\mu\nu;\alpha\beta} + v^{(0)}_{\mu\beta;\alpha\nu}\right) + \left[\sum_{\mu,\nu\neq\alpha} r^{(1)}_{\alpha\mu} r^{(1)}_{\alpha\nu} v^{(0)}_{\mu\beta;\nu\beta} + \alpha\leftrightarrow\beta\right] \; , \end{aligned} \tag{46}$$

and, to fourth order in $v^{(0)}$

$$
\begin{aligned}
v_{\alpha\beta;\alpha\beta}\, v_{\alpha\beta;\alpha\beta} \;=\; & v^{(0)}_{\alpha\beta;\alpha\beta} v^{(0)}_{\alpha\beta;\alpha\beta} - 2\left[\sum_{\mu\neq\alpha} (r^{(1)}_{\alpha\mu})^2 v^{(0)}_{\alpha\beta;\alpha\beta} v^{(0)}_{\alpha\beta;\alpha\beta} + \alpha\leftrightarrow\beta\right] \\
& + \left[4\sum_{\mu\neq\alpha} v^{(0)}_{\alpha\beta;\alpha\beta} r^{(2)}_{\alpha\mu} v^{(0)}_{\mu\beta;\alpha\beta} + \alpha\leftrightarrow\beta\right] + \left[2\sum_{\mu,\nu\neq\alpha} v^{(0)}_{\alpha\beta;\alpha\beta} r^{(1)}_{\alpha\mu} r^{(1)}_{\alpha\nu} v^{(0)}_{\mu\beta;\nu\beta} + \alpha\leftrightarrow\beta\right] \\
& + 4\sum_{\mu\neq\alpha;\nu\neq\beta} v^{(0)}_{\alpha\beta;\alpha\beta} r^{(1)}_{\alpha\mu} r^{(1)}_{\beta\nu}\left(v^{(0)}_{\mu\nu;\alpha\beta} + v^{(0)}_{\mu\beta;\alpha\nu}\right) + \left[4\sum_{\mu,\nu\neq\alpha} r^{(1)}_{\alpha\mu} v^{(0)}_{\mu\beta;\alpha\beta} r^{(1)}_{\alpha\nu} v^{(0)}_{\nu\beta;\alpha\beta} + \alpha\leftrightarrow\beta\right] \\
& + 8\sum_{\mu\neq\alpha;\nu\neq\beta} r^{(1)}_{\alpha\mu} v^{(0)}_{\mu\beta;\alpha\beta} r^{(1)}_{\beta\nu} v^{(0)}_{\alpha\nu;\alpha\beta}\,. \qquad (47)
\end{aligned}
$$

2. *Average Values*

We first calculate the average HF matrix element in the ensemble (iii), the two–body Gaussian ensemble. For a diagonal HF matrix element $v_{\alpha\beta;\alpha\beta}$ we can rewrite Eq. (40) as

$$
v_{\alpha\beta;\alpha\beta} = v^{(0)}_{\alpha\beta;\alpha\beta} + 2\sum_{\mu\neq\alpha} r^{(1)}_{\alpha\mu} v^{(0)}_{\mu\beta;\alpha\beta} + 2\sum_{\mu\neq\beta} r^{(1)}_{\beta\mu} v^{(0)}_{\mu\alpha;\beta\alpha}\,, \qquad (48)
$$

where the third term on the r.h.s. is obtained from the second term by exchanging α and β. To find the mean value of $v_{\alpha\beta;\alpha\beta}$ from Eq. (48), we calculate for $\mu\neq\alpha$

$$
\begin{aligned}
\overline{v^{(0)}_{\mu\delta;\alpha\delta} v^{(0)}_{\mu\beta;\alpha\beta}} \;=\; & 2u^2(\delta_{\delta\beta} - \delta_{\delta\beta}\delta_{\alpha\beta}\delta_{\delta\alpha} + \delta_{\mu\beta}\delta_{\delta\mu}\delta_{\alpha\beta}\delta_{\delta\alpha} - \delta_{\mu\beta}\delta_{\delta\mu}\delta_{\delta\beta} \\
& + \delta_{\mu\alpha}\delta_{\delta\beta} - \delta_{\mu\beta}\delta_{\delta\alpha}\delta_{\alpha\mu} + \delta_{\mu\beta}\delta_{\delta\alpha}\delta_{\alpha\beta}\delta_{\delta\mu} - \delta_{\mu\alpha}\delta_{\delta\beta}\delta_{\alpha\beta}\delta_{\delta\mu}) \\
=\; & 2u^2(\delta_{\delta\beta} - \delta_{\delta\beta}\delta_{\alpha\beta} - \delta_{\mu\beta}\delta_{\delta\mu}\delta_{\delta\beta}) = 2u^2\delta_{\delta\beta}(1 - \delta_{\alpha\beta} - \delta_{\mu\beta})\,, \qquad (49)
\end{aligned}
$$

where all other terms vanish since $\mu\neq\alpha$. Averaging $v_{\alpha\beta;\alpha\beta}$ in Eq. (48) using Eq. (49), we find

$$
\begin{aligned}
\bar{v}_{\alpha\beta;\alpha\beta} \;=\; & \bar{v}^{(0)}_{\alpha\beta;\alpha\beta} + 4u^2(1-\delta_{\alpha\beta})\left[\Theta(n-\beta)\left(\sum_{\mu\neq\alpha}\frac{1}{\epsilon_\alpha - \epsilon_\mu} - \frac{1}{\epsilon_\alpha - \epsilon_\beta}\right) + \alpha\leftrightarrow\beta\right] \\
=\; & 4u^2(1-\delta_{\alpha\beta})\left[\Theta(n-\alpha)\sum_{\mu\neq\alpha,\beta}\frac{1}{\epsilon_\beta - \epsilon_\mu} + \Theta(n-\beta)\sum_{\mu\neq\alpha,\beta}\frac{1}{\epsilon_\alpha - \epsilon_\mu}\right]\,. \qquad (50)
\end{aligned}
$$

For a general matrix element $v_{\alpha\beta;\gamma\delta}$ we find

$$
\bar{v}_{\alpha\beta;\gamma\delta} = \left(\sum_{\mu\neq\alpha}\overline{r^{(1)}_{\alpha\mu} v^{(0)}_{\mu\beta;\gamma\delta}}\right) + (\alpha\leftrightarrow\beta,\gamma\leftrightarrow\delta) + (\alpha\leftrightarrow\gamma,\beta\leftrightarrow\delta) + (\alpha\leftrightarrow\delta,\beta\leftrightarrow\gamma)\,, \qquad (51)
$$

where we have used Eq. (40) and the symmetries of v. We have

$$
\begin{aligned}
\sum_{\mu\neq\alpha}\overline{r^{(1)}_{\alpha\mu} v^{(0)}_{\mu\beta;\gamma\delta}} \;=\; & \frac{1}{\epsilon_\alpha - \epsilon_\mu}\sum_\sigma \Theta(n-\sigma)\overline{v^{(0)}_{\mu\sigma;\alpha\sigma} v^{(0)}_{\mu\beta;\gamma\delta}}\,, \\
\overline{v^{(0)}_{\mu\sigma;\alpha\sigma} v^{(0)}_{\mu\beta;\gamma\delta}} \;=\; & 2u^2\delta_{\sigma\beta}(1-\delta_{\mu\beta})(\delta_{\alpha\gamma}\delta_{\sigma\delta} - \delta_{\alpha\delta}\delta_{\sigma\gamma})\,. \qquad (52)
\end{aligned}
$$

Using Eqs. (51) and (52), we find

$$
\bar{v}_{\alpha\beta;\gamma\delta} = (\delta_{\alpha\gamma}\delta_{\beta\delta} - \delta_{\alpha\delta}\delta_{\beta\gamma})\bar{v}_{\alpha\beta;\alpha\beta}\,, \qquad (53)
$$

where $\bar{v}_{\alpha\beta;\alpha\beta}$ is given by Eq. (50).

A similar calculation for the orthogonal ensemble (ii) yields for the average HF matrix element

$$\bar{v}_{\alpha\beta;\alpha\beta} = 6u^2(1-\delta_{\alpha\beta})\left[\Theta(n-\alpha)\sum_{\mu\neq\alpha,\beta}\frac{1}{\epsilon_\beta-\epsilon_\mu}+\Theta(n-\beta)\sum_{\mu\neq\alpha,\beta}\frac{1}{\epsilon_\alpha-\epsilon_\mu}\right]. \tag{54}$$

Comparing this with Eq. (50) we see that the result is the same as for the two–body Gaussian ensemble (iii) except for an overall factor of 3/2.

3. Variance

The expectation values of each of the seven terms on the r.h.s. of Eq. (47) can be calculated using Wick's theorem and Eq. (22). The calculation proceeds along lines similar to those of the previous Section. We do not give any details of this rather lengthy calculation and confine ourselves to the result. For the variance of the diagonal HF matrix elements we find

$$\sigma^2(v_{\alpha\beta;\alpha\beta}) = 4u^2(1-\delta_{\alpha\beta})\left[1-4u^2\Theta(n-\alpha)\sum_{\mu\neq\alpha,\beta}\frac{1}{(\epsilon_\beta-\epsilon_\mu)^2}-4u^2\Theta(n-\beta)\sum_{\mu\neq\alpha,\beta}\frac{1}{(\epsilon_\alpha-\epsilon_\mu)^2}\right]. \tag{55}$$

We observe that in contrast to the expressions derived for the average values of the matrix elements, Eq. (55) cannot be averaged over the GOE spectrum. This is because the integrals over the eigenvalues possess a logarithmic singularity. We shall return to this point when we compare the numerical results with the perturbative expressions in Section III C 3.

C. Statistics of the Hartree-Fock matrix elements: numerical results

We now report on numerical results concerning the statistics of the interaction matrix elements in the self–consistent HF basis, using the true random–matrix ensembles of Section II. We focus attention on the diagonal matrix elements $v_{\sigma\tau;\sigma\tau}$. Unless otherwise stated, we use in this Section the orthogonal "non-local" two–body ensemble (22) with $m = 30$ single–particle states and $n = 10$ electrons.

In the simulations, we construct the ensemble (3) as follows. We generate an $m \times m$ GOE matrix $h^{(0)}$ and diagonalize it to find its spectrum ϵ_α. We also generate Gaussian variables $v_{\alpha\beta;\gamma\delta}$ that are uncorrelated with the ϵ_α's and satisfy Eq. (20). We then compute the corresponding antisymmetrized interaction matrix elements from $v^A_{\alpha\beta;\gamma\delta} = v_{\alpha\beta;\gamma\delta} - v_{\alpha\beta;\delta\gamma}$.

The parameters of the ensemble are Δ and u. We have chosen the variance of the off–diagonal matrix elements of the GOE matrix $h^{(0)}$ to be $\sigma^2(h^{(0)}_{\alpha\beta}) = 3m/4\pi^2$, so that the mean level spacing in the middle of the spectrum is fixed at $\Delta = \sqrt{3}/2 \approx 0.866$. For each of the quantities presented in the figures of this Section we have used $10,000$ realizations.

In some of the calculations presented below, the single–particle spectrum is kept fixed and an ensemble of antisymmetrized two–body interaction matrix elements $v^A_{\alpha\beta;\gamma\delta}$ is generated as discussed above.

We used a rather low–dimensional GOE matrix to generate the one–body ensemble. An alternative choice would have been to use the center section of a high–dimensional GOE matrix as our starting point. Our choice has the obvious disadvantage of being not free of edge effects. However, the comparison made below of some of our results with those obtained from a picket–fence spectrum (constant spacings) shows that edge effects are small for the quantities we investigate. Our choice has the obvious advantage of keeping the dimension of all relevant matrices small. This is very useful in view of the number of realizations we have chosen, and of the need to perform a HF iteration for each of these realizations.

1. Distributions

We first consider the case of a fixed single–particle spectrum, allowing only the single–particle wave functions and, thus, the two–body matrix elements to vary randomly. For each realization of the two–body matrix elements, we solve the HF equations and compute the diagonal matrix elements $v_{\alpha\beta;\alpha\beta}$ in the HF single–particle basis.

Fig. 1 shows the distributions of three diagonal matrix elements $v_{\alpha\beta;\alpha\beta}$ for $n = 10$ electrons and $u = 0.1$. For $\alpha = 5, \beta = 5$ both levels are filled, for $\alpha = 5, \beta = 20$ one level is filled, the other is empty, and for $\alpha = 20, \beta = 20$, both levels are empty. The distributions are all well described by Gaussians (solid lines). The same holds true for the distributions generated by choosing both single–

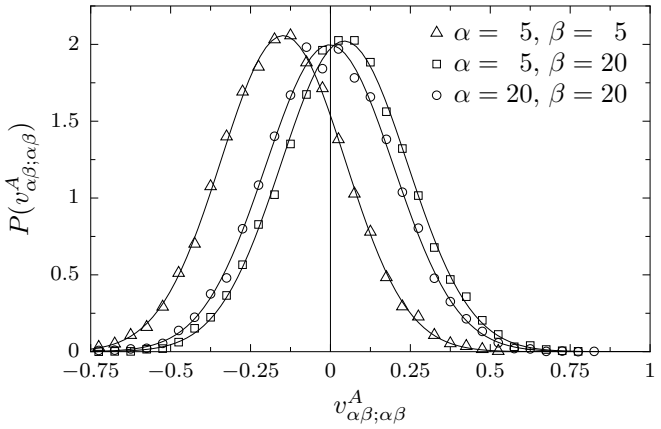

FIG. 1: The distributions $P(v_{\alpha\beta;\alpha\beta})$ of three diagonal matrix elements in the HF basis for a fixed single–particle GOE spectrum in the ensemble (22) with $u = 0.1$. There are $n = 10$ electrons. The symbols denote the results of the numerical simulations. The solid lines are Gaussian fits.

particle energies and two–body matrix elements at random. It is, thus, sufficient in all cases to consider only the first two moments of $v_{\alpha\beta;\alpha\beta}$.

2. Average HF matrix elements

The top two panels (a) and (b) of Fig. 2 show the average values of some diagonal matrix elements calculated for a fixed single–particle spectrum. This fixed spectrum was chosen as a picket–fence spectrum (equal spacings) in panel (a) of Fig. 2 and as a GOE spectrum in panel (b) of Fig. 2. The perturbative expression (50) shown by solid, dashed and dashed–dotted lines is in good agreement with the numerical results. The agreement is better for a picket–fence spectrum than for a GOE spectrum.

We turn to the general case where the statistics are collected by varying both the single–particle GOE spectrum and the single–particle wave functions. Such fully averaged HF matrix elements are shown in panel (c) of Fig. 2.

According to the perturbative expression (50), the full ensemble average of a HF diagonal matrix element is given by $4u^2(1-\delta_{\alpha\beta})C_{\alpha\beta}$ with

$$C_{\alpha\beta} = \left[\Theta(n-\alpha)\left\langle \sum_{\mu\neq\alpha,\beta} \frac{1}{\epsilon_\beta - \epsilon_\mu}\right\rangle + \Theta(n-\beta)\left\langle \sum_{\mu\neq\alpha,\beta} \frac{1}{\epsilon_\alpha - \epsilon_\mu}\right\rangle\right] . \quad (56)$$

The symbol $\langle \ldots \rangle$ denotes the GOE average. In Fig. 3 we show a three–dimensional plot of $C_{\alpha\beta}$ versus α and β for $m = 30$ and $n = 10$.

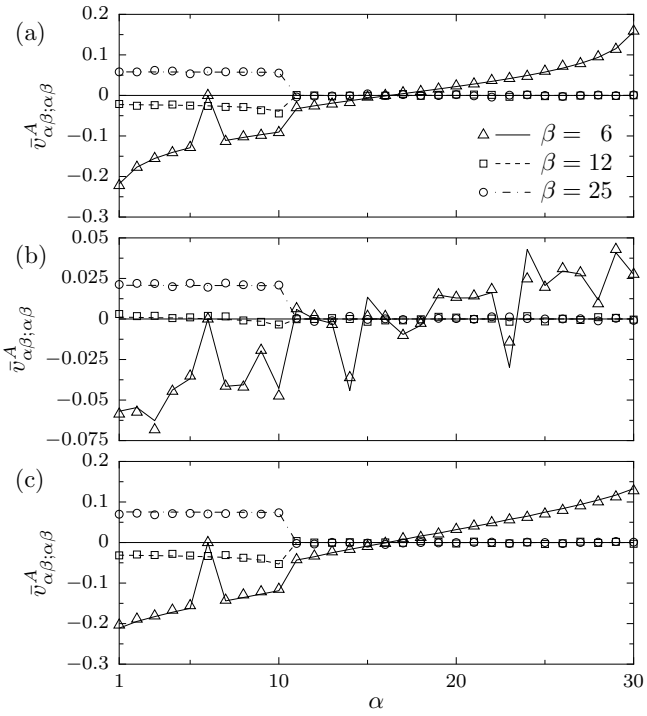

FIG. 2: Average matrix elements $\bar{v}_{\alpha\beta;\alpha\beta}$ in the HF basis versus α for fixed β. We show results for three values of β ($\beta = 6, 12, 25$). We use the ensemble (22) with $m = 30$ and for $n = 10$ electrons. (a) The data are generated for $u = 0.1$ and for a fixed picket–fence single–particle spectrum (equal spacings). The symbols give the numerical simulations, and the lines give the perturbative result (50). (b) As in panel (a) but for $u = 0.05$ and for a fixed single–particle GOE spectrum. (c) The results are for the same ensemble as in (a), but the average is taken over the full ensemble (22), i.e., over both the single–particle GOE spectrum and the two–body interaction matrix elements of Eq. (3). The symbols represent the numerical simulations and the lines the perturbative expression (50), averaged over the single–particle GOE spectrum.

For comparison, we show in Fig. 4 the full ensemble average of a diagonal HF matrix element (averaged numerically over both the two–body matrix elements and the single–particle GOE spectrum) versus α and β for $u = 0.1$. The result agrees well with $6u^2C_{\alpha\beta}$ if we take $C_{\alpha\beta}$ from Fig. 3.

3. Variance

The two–body matrix elements which serve as input in the HF calculation have a Gaussian distribution with second moments defined in Section II B 1. Our numerical simulations indicate that the variances σ^2 of the HF matrix elements are very close to these input values. We observe that in the HF basis σ decreases slightly, the size of the decrease depending on whether the diagonal matrix element corresponds to filled–filled, filled–empty

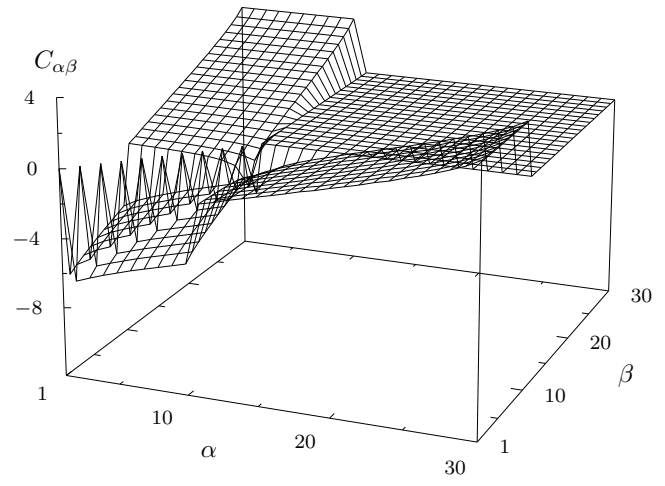

FIG. 3: Three–dimensional plot of $C_{\alpha\beta}$ [see Eq. (56)] versus α and β. The results shown are for $n = 10$ electrons occupying $m = 30$ orbitals.

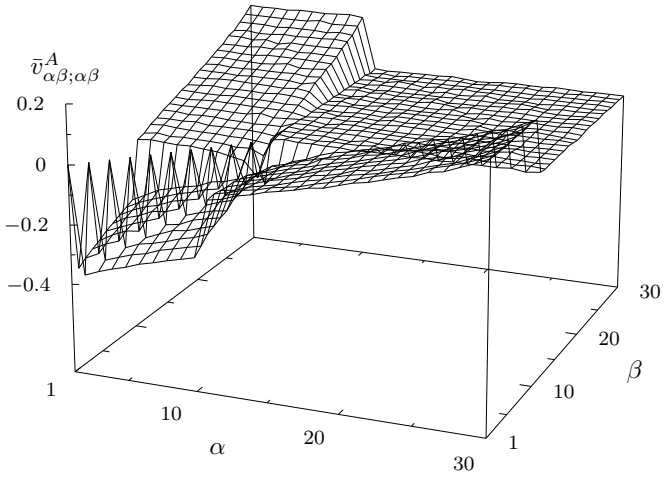

FIG. 4: Three–dimensional plot of the full ensemble average of $v_{\alpha\beta;\alpha\beta}$ versus α and β. We use the "local" interaction ensemble with $u = 0.1$ for $n = 10$ electrons occupying $m = 30$ orbitals. The results shown here agree well with the perturbative expression $6u^2 C_{\alpha\beta}$ where $C_{\alpha\beta}$ is shown in Fig. 3.

or empty–empty single–particle orbitals. There are fluctuations because of the finite size of the ensemble. To improve the statistics we further average the variances separately for these three different types of matrix elements. The top panel of Fig. 5 shows the resulting standard deviation $\sigma(v_{\alpha\beta;\alpha\beta})$ for the "local" interaction ensemble (17) versus u. The input value is $\sigma = \sqrt{6}u$. The difference between the HF results and the input value is amplified in the bottom panel of Fig. 5. The variance of the empty–empty matrix elements is practically unchanged, while the largest decrease is observed for the filled–filled matrix elements.

We have also compared our numerical results for a fixed choice of the single–particle spectrum with the perturbative expression (55). This expression seems to fail no matter how small u was chosen. (When u becomes too small, the statistical noise prohibits a meaningful comparison). While the numerical result is always close to $4u^2$, this is not true for the expression (55) which at times may even become negative. We speculate that this fact may signal a breakdown of perturbation theory but have not followed up this point.

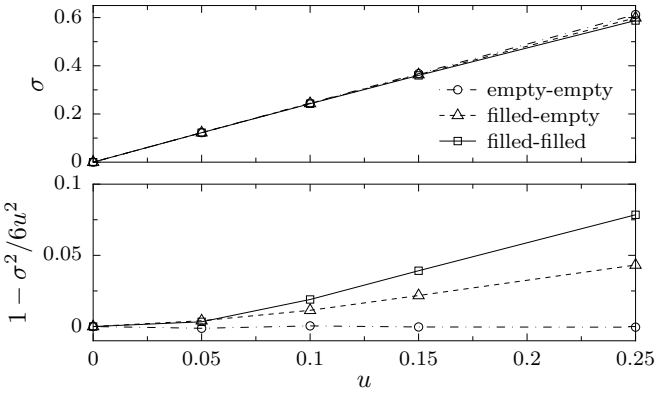

FIG. 5: Top panel: The standard deviation of a HF matrix element $\sigma(v_{\alpha\beta;\alpha\beta})$ versus u for the "local" interaction ensemble (17). We show results for three different types of diagonal matrix elements, corresponding to filled–filled, filled–empty and empty–empty single–particle levels. The results shown for each type are averaged over all matrix elements of that type. Bottom panel: The fractional deviation $1 - \sigma^2/6u^2$ of the variance σ^2 of the matrix elements in the HF basis from their variance $6u^2$ in the non–interacting basis versus u. Same conventions as in the top panel.

D. Statistics of the Hartree–Fock single–particle energies

The statistical results presented in the following are calculated for the entire ensemble, i.e., by collecting statistics over both the single–particle spectrum and the single–particle wave functions (i.e., the interaction matrix elements). Unless stated otherwise, the number of realizations used in the numerical simulations is $10,000$ (for each value of u).

The mean level spacing Δ of the single–particle GOE levels is given approximately by the inverse semi–circle law and increases towards the edges of the spectrum. We now consider the mean level spacing $\Delta_{\rm HF}$ of the HF single–particle spectrum calculated by averaging over the entire ensemble. Not surprisingly, we find that $\Delta_{\rm HF}$ increases monotonically with u. Fig. 6 shows $\Delta_{\rm HF}$ versus the level index α for different values of u. The solid line

is the GOE result. We notice the large peak at $n = 10$. It is due to a large spacing between the highest filled and the lowest empty HF level. This is a well–known feature of HF calculations and is referred to as the HF gap. We notice also the slight increase in the mean spacing close to the HF gap. In our discussion of the statistics of the HF single–particle energies $\epsilon_\alpha^{(n)}$, we treat filled levels, empty levels and the HF gap separately.

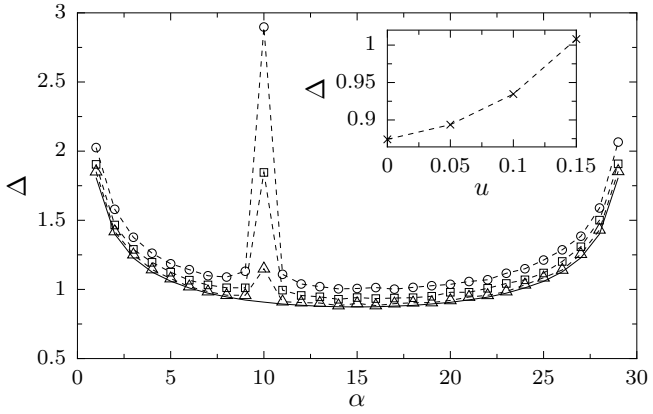

FIG. 6: The mean level spacing $\Delta_{\rm HF}$ of the single–particle HF levels versus level index α for $u = 0.05$ (triangles), $u = 0.1$ (squares) and $u = 0.15$ (circles). The results shown are for $n = 10$ electrons and $m = 30$ single–particle states. The solid line describes the mean level spacing Δ for a GOE of dimension $m = 30$. Inset: the mean level spacing in the center of the spectrum versus u.

1. Filled levels and empty levels

Let s denote the spacing of a pair of successive filled or empty levels, measured in units of the local mean level spacing. The nearest–neighbor spacing distribution $P(s)$ is found to follow the GOE Wigner distribution. We observe such behavior even for the pair of filled (empty) levels closest to the HF gap. This is demonstrated in Fig. 7 where the numerical distributions (histograms) for $P(s)$ are compared with the Wigner distribution (dashed lines) for different values of u and for both the highest two filled HF levels (top panels) and the lowest two empty HF levels (bottom panels).

2. Hartree–Fock gap

We simplify the notation by writing $v_{\alpha\beta} \equiv v_{\alpha\beta;\alpha\beta}$. In the HF basis and for n electrons, the HF gap is given by

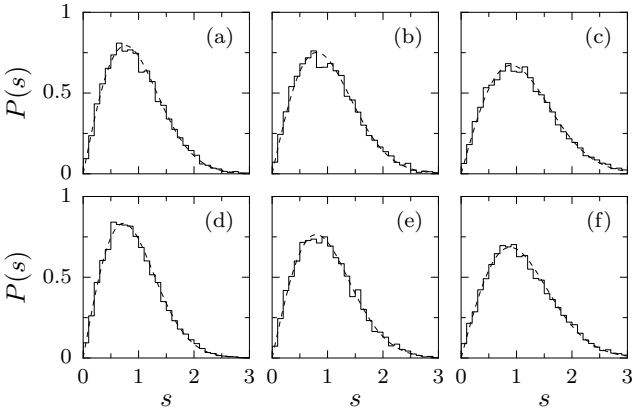

FIG. 7: Nearest–neighbor spacing distribution $P(s)$ versus spacing s where s is measured in units of the local mean level spacing of the corresponding HF levels. Top panel: The histograms show $P(s)$ for the highest two filled single–particle HF levels $\epsilon_{n-1}^{(n)}$ and $\epsilon_n^{(n)}$ (with $s = (\epsilon_n^{(n)} - \epsilon_{n-1}^{(n)})/\langle \epsilon_n^{(n)} - \epsilon_{n-1}^{(n)} \rangle$), and for three values of u: (a) $u = 0.05$; (b) $u = 0.1$; and (c) $u = 0.15$. The dashed lines give the GOE Wigner distribution. Bottom panels: same as in the top panels but for the two lowest empty single–particle HF levels $\epsilon_{n+1}^{(n)}$ and $\epsilon_{n+2}^{(n)}$. The values of u are (d) $u = 0.05$; (e) $u = 0.1$; and (f) $u = 0.15$.

$$\epsilon_{n+1}^{(n)} - \epsilon_n^{(n)} = (h_{n+1,n+1}^{(0)} - h_{n,n}^{(0)}) + v_{n+1,n} + \sum_{\tau=1}^{n-1} (v_{n+1,\tau} - v_{n,\tau}) \; . \tag{57}$$

The squares in the top panel of Fig. 8 show the numerical results for the average gap, calculated from the full ensemble (3) with a "local" interaction [Eq. (17)]. To estimate the average gap, we use in Eq. (57) the perturbative expression (54) for the diagonal HF matrix elements which we average over a single–particle GOE spectrum (see $C_{\alpha\beta}$ in Section III C). We also need to know the average values of $h_{n+1,n+1}^{(0)} - h_{n,n}^{(0)}$ which are found to be $0.895, 0.868, 0.836$, and 0.765 for $u = 0.05, 0.1, 0.15$ and 0.25, respectively (the corresponding value in the absence of the two–body interaction is $\Delta = 0.908$). The resulting estimate for the average gap depends quadratically on u, and is shown by the dotted–dashed line in the top panel of Fig. 8. For small values of u ($\lesssim 0.15$) our estimate provides a good approximation for the average HF gap, but for larger values there are deviations, indicating the breakdown of the lowest–order perturbative approach. We note that the average interaction (7) contributes a constant v_0 to the average gap. In our calculations we have set the average interaction to zero, and this constant (but large) contribution to the average gap is not shown in our numerical results.

The distribution $P(s)$ of the HF gap, shifted by its average value, is shown in Fig. 9 for several values of u (histograms). In Section IV A, we motivate an approxima-

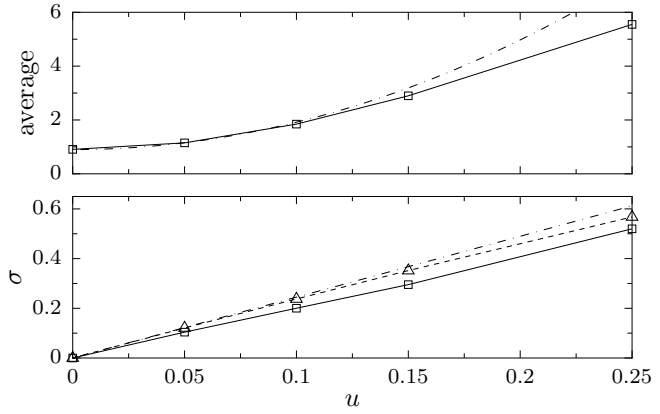

FIG. 8: Top panel: average HF gap versus u. The squares are the results of simulations of the full ensemble (3). The dotted–dashed line is obtained by using Eq. (57) and a spectral GOE average of the perturbative expression (50). Bottom panel: the squares depict the width σ of a Gaussian the convolution of which with a Wigner distribution is fitted to the gap distributions in Fig. 9. The dotted–dashed line is $\sqrt{6}u$, and the triangles (connected by the dashed line) are the standard deviations $\sigma(v_{n+1,n})$ of the corresponding HF interaction matrix element (see text).

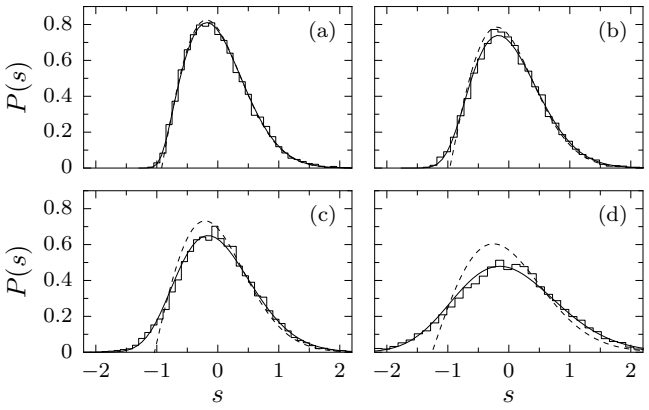

FIG. 9: The calculated distribution of the shifted HF gap (histograms) for four values of u: (a) $u = 0.05$; (b) $u = 0.1$; (c) $u = 0.15$; and (d) $u = 0.25$. The gap is shifted to have the average value zero. The solid lines describe convolutions of a shifted Wigner distribution (with an appropriate Δ) with a Gaussian. The width of the Gaussian is fitted. The dashed lines are the shifted Wigner distributions.

tion to this gap distribution as a convolution of a (shifted) Wigner distribution with an appropriate Δ, and a Gaussian. The dashed lines in Fig. 9 are the corresponding Wigner distributions, while the solid lines describe the convolutions for which the width σ of the Gaussian is fitted. This fitted value of σ is shown in the bottom panel of Fig. 8 versus u (squares). The dotted–dashed line in Fig. 8 is the input value $\sqrt{6}u$ for the standard deviation of a diagonal matrix element. The triangles give the standard deviation $\sigma(v_{n+1,n})$ of the diagonal matrix element $v_{n+1,n}$ in the HF basis for n electrons. We observe that σ is somewhat smaller than the standard deviation of the corresponding HF interaction matrix element.

3. Spacing correlator

In Section III D 1 we have seen that the nearest–neighbor spacing distributions of both, the occupied and the empty HF states, follow RMT statistics. But what about the correlation between occupied and empty levels? In this Section we show that the HF gap modifies that correlation so that it differs from the RMT prediction. To that end, we define the spacing correlator

$$c_\alpha = \frac{\overline{s_\alpha s_{\alpha+2}} - \bar{s}_\alpha \bar{s}_{\alpha+2}}{\sigma(s_\alpha)\sigma(s_{\alpha+2})} \,, \qquad (58)$$

where $s_\alpha = \epsilon_\alpha^{(n)} - \epsilon_{\alpha-1}^{(n)}$ $(\alpha = 2, \ldots, m)$ are nearest–neighbor spacings and $\sigma(s_\alpha)$ is the standard deviation of s_α. For the HF ensemble, the correlator c_n measures the spacing correlation across the gap, i.e., the correlation between the highest spacing of the filled levels and the lowest spacing of the empty levels.

For the GOE, the correlator (58) is denoted by $C(r = 1; t = 0)$ and explicitly given in Ref. 38. The correlator is negative and approximated by $C(r = 1, t = 0) \approx -1/[4\pi^2(4/\pi - 1)] \approx -0.093$. A more accurate numerical value is -0.087.

In the HF approach, the correlator (58) is small and exhibits large sample–to–sample fluctuations. Thus, a large number of realizations is required to obtain a reliable value. Table I shows c_n of the HF single–particle spectrum for several values of u. The results were obtained using 50,000 realizations (for each u) of the "local" interaction ensemble with $m = 30$. We observe that the correlator is negative and its magnitude becomes smaller as u increases. Hence the HF gap has the effect of weakening the correlation between filled and empty levels.

u	correlator c_n
0	-0.084 ± 0.011
0.05	-0.078 ± 0.011
0.10	-0.061 ± 0.012
0.15	-0.048 ± 0.011
0.25	-0.027 ± 0.013

TABLE I: The spacing correlator c_n across the HF gap for several values of u (using 50,000 realizations for each u).

On the other hand, when both spacings are between filled states ($\alpha \leq n - 2$) or both between empty states ($\alpha \geq n + 2$), we find that c_α is close to its standard GOE value (except for edge effects). This provides additional

support for the hypothesis that the filled and the empty HF states separately satisfy RMT statistics.

Fig. 10 demonstrates the behavior of the correlator c_α as a function of α for $u = 0.1$ and $u = 0.25$. For $\alpha \leq n-2$ and $\alpha \geq n+2$, c_α fluctuates around its RMT value. However, the correlator c_n between spacings on opposite sides of the gap decreases in magnitude with u, while the correlators c_{n-1} and c_{n+1} (for which one of the spacings is the gap itself) are enhanced in magnitude compared with the RMT value.

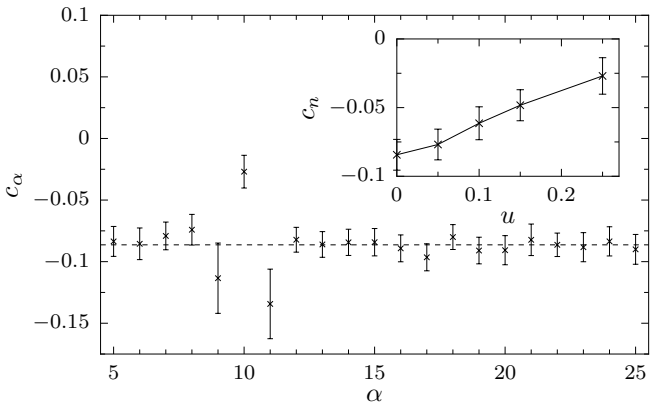

FIG. 10: The spacing correlator c_α [see Eq. (58)] versus α for the HF spectrum of the "local" interaction ensemble with $u = 0.25$ and $m = 30$ (values of α near the edges of the spectrum are omitted). The results shown are calculated for 50,000 realizations of the ensemble and include statistical errors. The dashed line is the GOE value of the correlator -0.0863 ± 0.0008 calculated from 500,000 realizations and averaged over α. Inset: the correlator c_n across the gap versus u.

E. Statistics of the Hartree-Fock single–particle wave functions

The induced ensemble is invariant under orthogonal (unitary) transformations of the single–particle basis. We show now that the corresponding single–particle HF ensemble is also invariant under orthogonal (unitary) transformations. For simplicity, we present the proof for the orthogonal case only.

We consider a particular realization (2) of the induced ensemble in a fixed basis $|i\rangle$. Under an orthogonal transformation $\hat{O}$ of the single–particle space with $a_i^\dagger \to \hat{O} a_i^\dagger \hat{O} = \sum_{i'} a_{i'}^\dagger O_{i'i}$, we obtain a new realization of the many–body ensemble,

$$H \to \tilde{H} = \hat{O} H \hat{O}^{-1} = \sum_{ij} \tilde{h}_{ij}^{(0)} a_i^\dagger a_j + \frac{1}{4} \sum_{ij;kl} \tilde{v}_{ij;kl}^A a_i^\dagger a_j^\dagger a_l a_k \ , \tag{59}$$

where the new single–particle Hamiltonian $\tilde{h}^{(0)}$ and interaction matrix elements $\tilde{v}^A$ are related to $h^{(0)}$ and v^A by

$$\begin{aligned} \tilde{h}_{ik}^{(0)} &= \sum_{jl} O_{ij} h_{jl}^{(0)} (O^{-1})_{lk} \ ; \\ \tilde{v}_{ij;kl}^A &= \sum_{i'j'k'l'} O_{ii'} O_{jj'} v_{i'j';k'l'}^A (O^{-1})_{k'k} (O^{-1})_{l'l} \ . \end{aligned} \tag{60}$$

The Hamiltonians $h^{(0)}$ and $\tilde{h}^{(0)}$ have identical single–particle spectra but different single–particle eigenstates. Both are members of the single–particle GOE. Likewise, the Hamiltonians H and $\tilde{H}$ are both members of the induced many–body ensemble.

In the fixed basis the single–particle HF Hamiltonian (32) has the form

$$h_{ik} = h_{ik}^{(0)} + \sum_{jl} v_{ij;kp}^A \rho_{pj} \ . \tag{61}$$

Here $\rho_{pj} = \langle j|\hat{\rho}|p\rangle = \sum_l \psi_l^*(p)\psi_l(j)$ is the matrix representation of the single–particle density operator $\hat{\rho} = \sum_{l=1}^n |\psi_l\rangle\langle\psi_l|$. As in Eq. (33), $|\psi_l\rangle$ denotes the l^{th} HF single–particle eigenstate, $\psi_l(j)$ its projection onto the fixed basis state j, and the sum is over the lowest n HF levels. We consider the transformed single–particle Hamiltonian

$$\tilde{h}_{ik} = \sum_{jl} O_{ij} h_{jl} (O^{-1})_{lk} \ . \tag{62}$$

To prove the orthogonal invariance of the ensemble of HF single–particle Hamiltonians, we have to show that $\tilde{h}$ is the HF Hamiltonian for the new realization (59) of the many–body ensemble. Using Eq. (61) we can write $\tilde{h}$ as

$$\tilde{h}_{ik} = \tilde{h}_{ik}^{(0)} + \sum_{jl} \tilde{v}_{ij;kl}^A \tilde{\rho}_{lj} \ , \tag{63}$$

where

$$\hat{\tilde{\rho}} = \hat{O} \rho \hat{O}^{-1} = \sum_{l=1}^n |\tilde{\psi}_l\rangle\langle\tilde{\psi}_l| \ , \ \text{with } |\tilde{\psi}_l\rangle = \hat{O}|\psi_l\rangle \ . \tag{64}$$

This shows that $\tilde{h}_{ik}$ is indeed the HF Hamiltonian of the realization (59) provided that $\hat{\tilde{\rho}}$ is the density matrix of the lowest n eigenstates of $\tilde{h}$. But Eq. (62) shows that $\tilde{h}$ has the same eigenvalues $\epsilon_l^{(n)}$ as h and that the eigenvectors of $\tilde{h}$ are given by the second of Eqs. (64). This completes the proof. We conclude that the invariance of the many–body ensemble under orthogonal transformations implies the orthogonal invariance of the HF ensemble. In the GOE, the statistics of the eigenvectors are determined by the orthogonal invariance of the ensemble. Thus we expect the eigenvectors of the HF ensemble to obey the same statistics. For example, the distribution of the components $\psi_l(j)$ of the HF eigenvector $|\psi_l\rangle$ in the fixed basis of states $|j\rangle$ must depend on orthogonal invariants only. For a single eigenvector the only such

orthogonal invariant is $\sum_j \psi_l^2(j)$. Since the eigenvector is normalized to unity, the probability density is

$$P(\psi_l(1), \psi_l(2), \ldots) \propto \delta(\sum_j \psi_l^2(j) - 1) \; . \qquad (65)$$

As for the GOE, integrating over all components except the j-th, we find

$$P(\psi_l(j)) = \pi^{-1/2} \frac{\Gamma(\frac{m}{2})}{\Gamma(\frac{m-1}{2})} [1 - \psi_l^2(j)]^{\frac{m-3}{2}} \; , \qquad (66)$$

where m is the dimension of the single–particle space. In the limit of large m, $P(\psi_l(j))$ can be approximated by a Gaussian, $P(\psi_l(j)) \propto e^{-m\psi_l^2(j)/2}$.

We have computed numerically the statistics of an HF eigenfunction component in the "local" interaction orthogonal ensemble (17). Since there is an ambiguity of the overall sign of the wave function, we have calculated the distribution of $y = m\psi_l^2(j)$ (the normalization is chosen to satisfy $\bar{y} = 1$). It follows from (66) that

$$P(y) = \pi^{-1/2} \frac{\Gamma(\frac{m}{2})}{\Gamma(\frac{m-1}{2})} (my)^{-1/2} \left(1 - \frac{y}{m}\right)^{\frac{m-3}{2}} \; . \qquad (67)$$

In the limit of large m, this is just the Porter–Thomas distribution

$$P(y) = (2\pi y)^{-1/2} e^{-y/2} \; . \qquad (68)$$

Fig. 11 shows numerical results for the distribution of $P(\ln y)$ versus $\ln y$ for an HF eigenstate in the middle of the spectrum and for $m = 30$. Since the distribution is independent of the particular component, we collect statistics from all components. Results are shown for $u = 0.05, 0.1, 0.15$ and 0.25 (symbols). For all values of u the distributions are well described by Eq. (67) (solid line). For reference we also show the Porter–Thomas distribution (dashed line). The observed small deviation from the limiting case of a Porter–Thomas distribution is a finite–size effect.

As in the GOE, it is also possible to calculate from Eq. (65) the correlator for two different squared components of an HF eigenfunction,

$$\frac{\overline{\psi_l^2(i)\psi_l^2(j)} - \overline{\psi_l^2(i)}\;\overline{\psi_l^2(j)}}{\sigma(\psi_l^2(i))\sigma(\psi_l^2(j))} = -\frac{1}{m-1} \; , \qquad (69)$$

where $\sigma^2(\psi_l^2(i))$ is the variance of $\psi_l^2(i)$. This correlator is rather small and in the numerical simulations exhibits large fluctuations. However, on average it agrees with the analytical result Eq. (69).

In Sections III D and III E, we have thus shown that the fluctuation properties of the HF ensemble are very close to those of RMT: The single–particle HF wave functions obey the same statistics, and the single–particle HF eigenvalues do, too, except near the HF gap which plays a special role in the spectrum. The correlations between filled and empty levels are weakened by the gap.

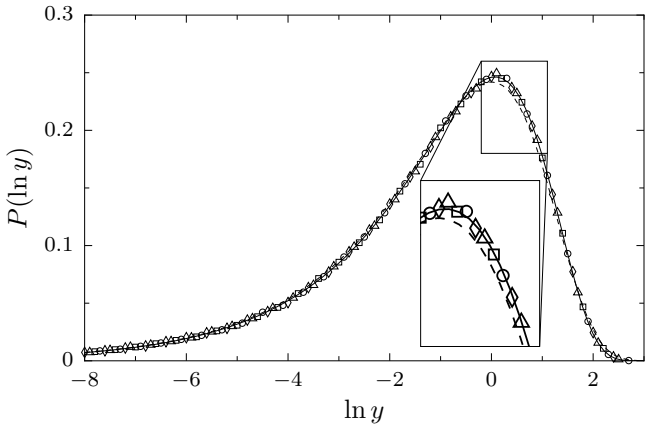

FIG. 11: The distributions $P(\ln y)$ versus $\ln y$, where y is the square of an HF wave function component (scaled to give $\bar{y} = 1$) for $u = 0.05$ (triangles), $u = 0.1$ (squares), $u = 0.15$ (circles) and $u = 0.25$ (diamonds). We use the "local" interaction orthogonal ensemble (17) with $m = 30$ and $n = 10$. The solid line is the finite–m RMT distribution (67) and the dashed line is the Porter–Thomas distribution (68). A section of the graph is magnified to render more details.

IV. HARTREE–FOCK APPROACH TO DISORDERED SYSTEMS: ADDITION OF ELECTRONS

In the HF approximation, the many–particle ground–state energy $E_{\rm HF}(n)$ of n electrons can be written in several ways. In an arbitrary fixed single–particle basis, we have

$$E_{\rm HF}(n) = \sum_{\alpha\gamma} h^{(0)}_{\alpha\gamma} \rho_{\gamma\alpha} + \frac{1}{2} \sum_{\substack{\alpha\gamma \\ \beta\delta}} \rho_{\gamma\alpha} v_{\alpha\beta;\gamma\delta} \rho_{\delta\beta} \; , \qquad (70)$$

where ρ is the self–consistent density matrix of Eq. (33).

An alternative expression (in terms of the single–particle HF energies) is

$$E_{\rm HF}(n) = \sum_{\alpha=1}^{n} \epsilon_\alpha^{(n)} - \frac{1}{2} \sum_{\substack{\alpha\gamma \\ \beta\delta}} \rho_{\gamma\alpha} v_{\alpha\beta;\gamma\delta} \rho_{\delta\beta} \; , \qquad (71)$$

where the double counting of the interaction terms (in the sum of the single–particle HF energies) is corrected by the second term on the r.h.s. of Eq. (71). Both of these expressions simplify when written in the HF basis [in which $\rho_{\gamma\alpha} = \delta_{\alpha\gamma}\Theta(n - \alpha)$]

$$\begin{aligned} E_{\rm HF}(n) &= \sum_{\alpha=1}^{n} h^{(0)}_{\alpha\alpha} + \frac{1}{2} \sum_{\alpha,\beta=1}^{n} v_{\alpha\beta;\alpha\beta} \\ &= \sum_{\alpha=1}^{n} \epsilon_\alpha^{(n)} - \frac{1}{2} \sum_{\alpha,\beta=1}^{n} v_{\alpha\beta;\alpha\beta} \; . \end{aligned} \qquad (72)$$

A. Peak spacing distribution

The position (as given by the gate voltage) of a Coulomb–blockade peak at low temperature is indicative of the change in the ground–state energy of a quantum dot due to the addition of an electron (known as the addition energy). The spacing Δ_2 between successive Coulomb–blockade peaks (for short: the peak spacing) is then given by the second–order difference of the ground–state energies versus particle number. In the HF approximation we have

$$\Delta_2 \approx E_{\rm HF}(n+1) + E_{\rm HF}(n-1) - 2E_{\rm HF}(n) \; . \qquad (73)$$

In the CI model, i.e., when only the average interaction is taken into account, $\Delta_2 = (\epsilon_{n+1} - \epsilon_n) + v_0$, and the distribution of Δ_2 is a shifted Wigner distribution. Experimentally, the distribution is closer to a Gaussian,[5,6,7] and this was understood to be a residual interaction effect.

The histograms in Fig. 12 show $P(\Delta_2 - \bar{\Delta}_2)$ in the HF approximation for the same cases as in Fig. 9. The solid lines are again convolutions of a Wigner distribution with a Gaussian of width σ for the spacing distribution (this will be motivated in the following Section). The fitted values of σ are shown versus u as squares in Fig. 13. The dotted–dashed line, triangles, and dashed line are the same as in Fig. 8. We note that the average interaction contributes to Δ_2.

In the spinless case, the average interaction is given by Eq. (7), contributing a constant v_0 to Δ_2, which is canceled out in $\Delta_2 - \bar{\Delta}_2$. Thus the distribution $P(\Delta_2 - \bar{\Delta}_2)$ is not affected by the average interaction. This would no longer be true if spin were included: The average interaction in Eq. (9) has additional terms (i.e., an exchange interaction, and, in the orthogonal case, a Cooper channel interaction), which are not constant for a fixed number of electrons.

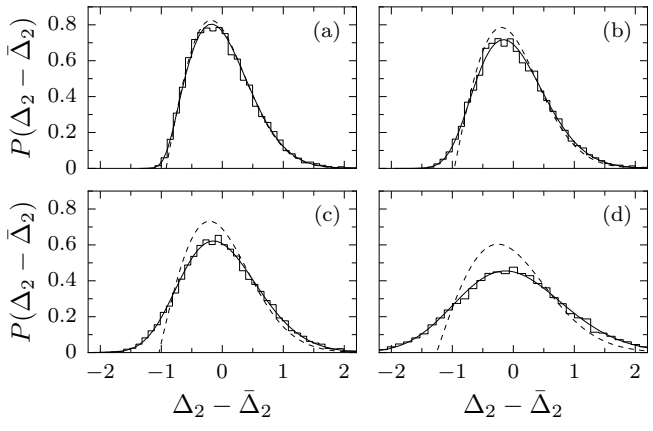

FIG. 12: Peak spacing distribution $P(\Delta_2 - \bar{\Delta}_2)$ for the same set of u–values as in Fig. 9.

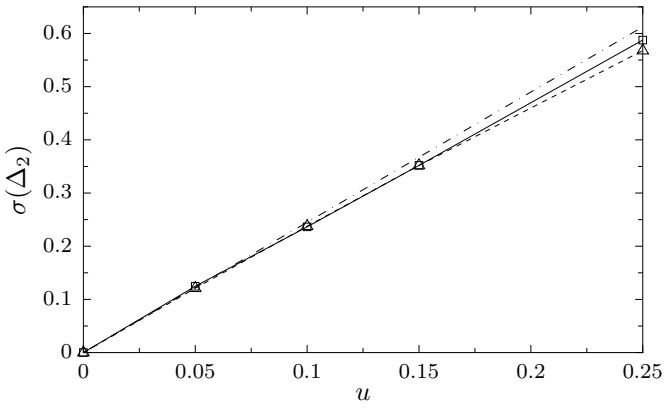

FIG. 13: The squares depict the width σ of a Gaussian the convolution of which with a Wigner distribution is fitted to the peak spacing distribution $P(\Delta_2 - \bar{\Delta}_2)$ in Fig. 12. Dotted–dashed line, triangles, and dashed line are as in Fig. 8.

B. Koopmans' approach

As an electron is added to the quantum dot, the self–consistent single–particle HF wave functions are expected to change. In Koopmans' limit, this change is neglected.[33] This assumption implies predictions for the peak–spacing distribution which we now test.

We first calculate the addition energy $E_{\rm HF}(n+1) - E_{\rm HF}(n)$ in Koopmans' limit. We use the HF wave functions for n electrons to write expressions for $E_{\rm HF}(n)$ and $E_{\rm HF}(n+1)$. For $E_{\rm HF}(n)$ we use the exact HF relation $E_{\rm HF}(n) = \sum_{\alpha=1}^{n} h^{(0)}_{\alpha\alpha} + \frac{1}{2}\sum_{\alpha\beta=1}^{n} v_{\alpha\beta}$. Using the same single–particle wave functions, we write for $E_{\rm HF}(n+1)$ the approximate relation $E_{\rm HF}(n+1) \approx \sum_{\alpha=1}^{n+1} h^{(0)}_{\alpha\alpha} + \frac{1}{2}\sum_{\alpha\beta=1}^{n+1} v_{\alpha\beta}$. We obtain

$$E_{\rm HF}(n+1) - E_{\rm HF}(n) \approx h^{(0)}_{n+1,n+1} + \sum_{\beta=1}^{n+1} v_{n+1,\beta} = \epsilon^{(n)}_{n+1} \; . \qquad (74)$$

A similar expression can be obtained for the $n-1 \to n$ transition, i.e., $E_{\rm HF}(n) - E_{\rm HF}(n-1) \approx \epsilon^{(n-1)}_{n}$, where we have used the HF wave functions of $n-1$ electrons. We then find from Eq. (73) the approximate relation[9]

$$\begin{aligned} \Delta_2 \approx \epsilon^{(n)}_{n+1} - \epsilon^{(n-1)}_{n} &= (\epsilon^{(n)}_{n+1} - \epsilon^{(n-1)}_{n+1}) + (\epsilon^{(n-1)}_{n+1} - \epsilon^{(n-1)}_{n}) \\ &\approx v_{n+1,n} + s \; , \end{aligned} \qquad (75)$$

where $s = \epsilon^{(n-1)}_{n+1} - \epsilon^{(n-1)}_{n}$ is the spacing between the two lowest empty levels for $n-1$ electrons. In deriving the second approximate relation in Eq. (75), we have also used $\epsilon^{(n)}_{n+1} \approx \epsilon^{(n-1)}_{n+1}) + v_{n+1,n}$, an expression that follows from Koopmans' limit for the $n-1 \to n$ transition.

An expression analogous to Eq. (74) can be derived from the $n+1 \to n$ transition, assuming the single–

particle HF wave functions do no change upon the removal of an electron from the dot. Using the HF wave functions of $n+1$ electrons, we find

$$E_{\rm HF}(n+1) - E_{\rm HF}(n) \approx \epsilon_{n+1}^{(n+1)} \ . \qquad (76)$$

Applying a similar relation for the $n \to n-1$ transition, we find another expression for Δ_2,

$$\begin{aligned} \Delta_2 \approx \epsilon_{n+1}^{(n+1)} - \epsilon_n^{(n)} &= (\epsilon_{n+1}^{(n+1)} - \epsilon_n^{(n+1)}) + (\epsilon_n^{(n+1)} - \epsilon_n^{(n)}) \\ &\approx s + v_{n+1,n} \ , \end{aligned} \qquad (77)$$

where $s = \epsilon_{n+1}^{(n+1)} - \epsilon_n^{(n+1)}$ is the spacing between the two highest filled levels for $n+1$ electrons.

If the HF levels and HF interaction matrix elements are uncorrelated, Eqs. (75) and (77) suggest that the distribution of Δ_2 can be described by a convolution of a Wigner distribution (with Δ given by the average spacing of the two lowest empty or two highest filled levels in the dot, respectively), and a Gaussian whose width σ is given by the standard deviation of the HF matrix element $v_{n+1,n}$. The results shown in Fig. 12 confirm that the peak spacing distribution is well described by a convolution of a Wigner distribution with a Gaussian (Δ is determined from a mean level density that excludes the gap). Furthermore, for small values of u ($\lesssim 0.15$), the width of the Gaussian is well described by $\sigma(v_{n+1,n})$ (see Fig. 13). For larger values of u, we observe some deviations.

In view of Eqs. (75) and (77), it is interesting to compare directly the peak spacing distribution $P(\Delta_2)$ with the distributions $P(\epsilon_{n+1}^{(n+1)} - \epsilon_n^{(n)})$ and $P(\epsilon_{n+1}^{(n)} - \epsilon_n^{(n-1)})$ using the exact self–consistent single–particle HF energies (i.e., not using Koopmans' limit).[19] The results are shown in Fig. 14 for $u = 0.1$. Both $P(\epsilon_{n+1}^{(n+1)} - \epsilon_n^{(n)})$ and $P(\epsilon_{n+1}^{(n)} - \epsilon_n^{(n-1)})$ approximate $P(\Delta_2)$ very well.

If we use Koopmans' limit simultaneously for the addition and removal of an electron in an n–electron dot, i.e., for the transitions $n \to n+1$ and $n \to n-1$, we obtain the relation $\Delta_2 \approx \epsilon_{n+1}^{(n)} - \epsilon_n^{(n)}$. The quantity $\epsilon_{n+1}^{(n)} - \epsilon_n^{(n)}$ is just the gap in the n–electron dot. This fact motivates the description of the gap distribution in Fig. 9 as a convolution of a Wigner distribution with a Gaussian. The width σ of the Gaussian (found from the gap distribution) is rather close to $\sigma(v_{n+1,n})$ (see Fig. 8), although not as close as the value of σ found from the peak–spacing distribution (see Fig. 13).

In Fig. 14 we also compare the gap distribution $P(\epsilon_{n+1}^{(n)} - \epsilon_n^{(n)})$ with the peak–spacing distribution (without subtracting the average values of the respective quantities). We observe that the gap distribution is similar in shape to $P(\Delta_2)$ (both are convolutions of a Wigner distribution with a Gaussian) but is shifted to the right. This suggests that the approximation $\Delta_2 \approx \epsilon_{n+1}^{(n)} - \epsilon_n^{(n)}$ does not work as well as Eqs. (75) and (77), in particular for the average values.

The qualitative difference in the various approximations for Δ_2 can be explained as follows. The single–particle HF energies $\epsilon_{n+1}^{(n)}$ and $\epsilon_n^{(n-1)}$ in Eq. (75) correspond to empty levels and thus contain both HF matrix elements connecting empty and filled orbitals. The average values of these HF matrix elements are similar (see, e.g., in Fig. 2 and Eq. (54)) and cancel out when their differences are taken to find Δ_2. Similarly, the HF energies $\epsilon_{n+1}^{(n+1)}$ and $\epsilon_n^{(n)}$ in Eq. (77) both correspond to filled levels. Both contain HF matrix elements between two filled levels whose averages are again similar and cancel out upon taking their difference. Because of this cancellation effect, the approximations in Eqs. (75)and (77) work better than those in Eqs. (74)and (76), respectively. However, the gap is the difference between an empty level and a filled level ($\epsilon_{n+1}^{(n)}$ and $\epsilon_n^{(n)}$, respectively). The HF interaction matrix elements are of the type empty–filled for the empty level and filled–filled for the filled level. The average values of these different types of matrix elements are rather different and their differences contribute to the large average HF gap observed in Figs. 8 and 14. We note that both Δ_2 and the gap include a large additional constant v_0 (mostly charging energy) which is not shown in our numerical results (since we set the average interaction in the original ensemble to zero).

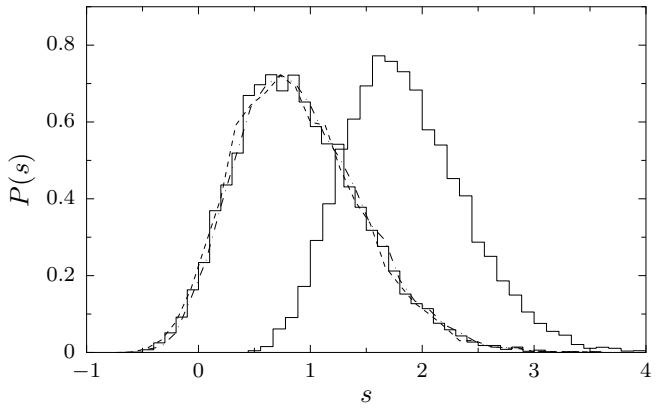

FIG. 14: The peak spacing distribution $P(\Delta_2)$ (left histogram) is compared with $P(\epsilon_{n+1}^{(n+1)} - \epsilon_n^{(n)})$ (dashed line), $P(\epsilon_{n+1}^{(n)} - \epsilon_n^{(n-1)})$ (dotted–dashed line) and the gap distribution (right histogram). The ensemble has $u = 0.1$.

Another motivation for comparing the peak–spacing distribution with the above three distributions (using in each case the exact HF levels for the appropriate number of electrons) is provided by inequalities for the addition energy that are exact in the HF approximation. The basic inequalities are[19]

$$\epsilon_{n+1}^{(n+1)} \le E_{\rm HF}(n+1) - E_{\rm HF}(n) \le \epsilon_{n+1}^{(n)} \ . \qquad (78)$$

Both inequalities follow from the variational principle for the HF ground–state energy. To obtain the right inequal-

ity, we use the variational principle for $n+1$ electrons. As a trial wave function we choose the Slater determinant of the lowest $n+1$ HF wave functions found in the exact HF solution for n electrons to obtain $E_{\rm HF}(n+1) \leq \sum_{\alpha=1}^{n+1} h^{(0)}_{\alpha\alpha} + \frac{1}{2}\sum_{\alpha\beta=1}^{n+1} v_{\alpha\beta}$. Combined with the exact relation $E_{\rm HF}(n) = \sum_{\alpha=1}^{n} h^{(0)}_{\alpha\alpha} + \frac{1}{2}\sum_{\alpha\beta=1}^{n} v_{\alpha\beta}$, we find the right inequality in (78). Similarly, the left inequality in (78) is obtained by using a trial Slater determinant composed of the lowest n orbitals found in the exact HF solution for $n+1$ electrons to put an upper bound on $E_{\rm HF}(n)$.

Rewriting (78) with n replaced by $n-1$, we obtain HF inequalities for the "removal" energy $E_{\rm HF}(n-1) - E_{\rm HF}(n)$

$$-\epsilon_n^{(n-1)} \leq E_{\rm HF}(n-1) - E_{\rm HF}(n) \leq -\epsilon_n^{(n)} \ . \qquad (79)$$

The peak spacing Δ_2 is obtained by summing the addition and removal energies in Eqs. (78) and (79). We find that the gap is an upper bound for Δ_2, i.e.,

$$\Delta_2 \leq \epsilon_{n+1}^{(n)} - \epsilon_n^{(n)} \ . \qquad (80)$$

This relation is consistent with the shift to the right of the gap distribution relative to the peak–spacing distribution (see Fig. 14). However, inspecting the inequalities in (78) and (79), we conclude that the quantities $\epsilon_{n+1}^{(n)} - \epsilon_n^{(n-1)}$ and $\epsilon_{n+1}^{(n+1)} - \epsilon_n^{(n)}$ are neither upper nor lower bounds for Δ_2. As discussed above, they turn out to be rather good approximations for Δ_2 (for $u \lesssim 0.15$).

C. The gap and peak–spacing distributions in the small u limit

In Sections III D 2 and IV A, we have shown that the gap and peak–spacing distributions can be approximated as convolutions of a Wigner distribution (evaluated with the HF mean–level spacing) and a Gaussian whose width σ is close to $\sigma(v_{n+1,n})$ (for the "local" interaction ensemble $\sigma(v_{n+1,n}) \approx \sqrt{6}u$). On might have chosen another approach: One may attempt to use Eq. (57) directly to infer the distribution of, e.g., the gap in the limit $u \to 0$. The various diagonal HF interaction matrix elements in Eq. (57) are approximately uncorrelated Gaussian variables with variance $\sigma^2(v_{n+1,n}) \approx 6u^2$ each. Furthermore, to first order in the interaction, we have $h^{(0)}_{\alpha,\alpha} \approx \epsilon_\alpha$ and $v_{\alpha,\beta} \approx v^{(0)}_{\alpha,\beta}$. Within RMT the quantities ϵ_α and $v^{(0)}_{\alpha,\beta}$ are uncorrelated. One might then conclude from Eq. (57) that, in the limit $u \to 0$, the gap distribution is a convolution of a Wigner distribution (evaluated with the GOE value of Δ without interaction) and a Gaussian whose width is $\approx \sigma = \sqrt{2n-1}\,\sigma(v^{(0)}_{n+1,n})\sqrt{6}u$ [there are $2n-1$ interaction matrix elements in Eq. (57)].

When compared with our previous results, the width σ of the Gaussian would then be enhanced by the large factor $\sqrt{2n-1}$. This increase is not compensated by the small decrease in the width of the Wigner distribution (the GOE value of Δ is a little smaller than the HF value $\Delta_{\rm HF}$). The result is a distribution which is much wider than the one found in the numerical simulation. We show in Fig. 15 the gap distribution $P(\Delta_2)$ (histogram) for a small value of u ($u = 0.05$). The solid line, predicted by Eq. (75) or Eq. (77), is a convolution of a Wigner distribution (with the appropriate Δ at $u = 0.05$) and a Gaussian with a width of $\sigma = \sigma(v^{(0)}_{n+1,n})$. As expected, the agreement is very good. However, the distribution that one infers using Eq. (57) in the limit $u \to 0$ (dashed line) is much broader. The discrepancy is due to the fact that even for very small values of u, the difference $h^{(0)}_{n+1,n+1} - h^{(0)}_{n,n}$ is strongly correlated with the HF matrix elements. Hence, the assumption made in using Eq. (57) is not correct. The inset of Fig. 15 shows the distribution of $h^{(0)}_{n+1,n+1} - h^{(0)}_{n,n}$ (histograms). This distribution can be approximately fitted by a Gaussian (solid line), but is distinctly different from the Wigner distribution of $\epsilon_{n+1} - \epsilon_n$ (dashed line).

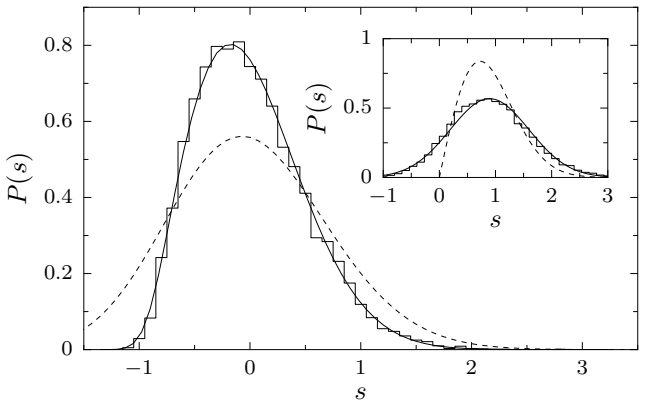

FIG. 15: The peak spacing distribution $P(\Delta_2)$ (histogram) for the "local" interaction ensemble with $u = 0.05$ is compared with a convolution of a Wigner distribution with a Gaussian whose width is $\sigma(v^{(0)}_{n+1,n})$ (solid line). The dashed line describes a convolution of a Wigner distribution and a Gaussian with a width of $\sqrt{2n-1}\ \sigma(v^{(0)}_{n+1,n})$. Inset: the distribution of $h^{(0)}_{n+1,n+1} - h^{(0)}_{n,n}$ (histogram) is approximately fitted by a Gaussian (solid line). The dashed line is the Wigner distribution of $\epsilon_{n+1} - \epsilon_n$. The number of electrons is $n = 10$.

D. Peak–height distribution

To measure the conductance, it is necessary to couple the dot to external leads. For weak coupling (i.e., for an almost isolated dot) and at low temperature ($T \ll \Delta$), the conductance peak height can be expressed in terms of the ground–state wave functions of the dot with n and $n+1$ electrons, and we can use the formalism developed here to study the statistical properties of the conductance. In

terms of the rates Γ^l and Γ^r for an electron to tunnel into the dot from the left and right leads, respectively, the peak height is given by

$$G \propto \frac{e^2}{\hbar k T} \frac{\Gamma^l \Gamma^r}{\Gamma^l + \Gamma^r} \ . \tag{81}$$

The rates are squares of partial–width amplitudes, $\Gamma^{l,r} = |\gamma^{l,r}|^2$. In the CI model, the γ's are proportional to the projection of a single–particle eigenfunction (occupied by the electron that tunnels into the dot) on the respective lead (or point contact $\mathbf{r}$). For symmetric leads that are separated by a distance large compared with the Fermi wavelength, the amplitudes γ^l and γ^r are uncorrelated Gaussian random variables with zero mean value and a common second moment. This leads to the well–known predictions for the peak–height distributions.[3]

A study of the peak height statistics in a small dot described by an Anderson model plus Coulomb interactions suggested that the peak–height distribution is only weakly affected by residual interactions.[39] To find out whether this result is generic, we use in the following the HF approximation to study the peak-height distribution within the framework of the induced two–body ensembles.

In the presence of interactions (beyond charging energy), we have

$$\gamma \propto \langle \Phi(n+1) | \hat{\psi}^\dagger(\mathbf{r}) | \Phi(n) \rangle \ , \tag{82}$$

where $\hat{\psi}^\dagger(\mathbf{r})$ creates an electron at the point contact $\mathbf{r}$, and $\Phi(n)$ is the ground–state wave function of the dot with n electrons. In the HF approximation, $\Phi(n)$ is a Slater determinant of the lowest n single–particle HF wave functions $\psi_1, \ldots, \psi_n$.

In Koopmans' limit, the single–particle HF wave functions do not change with n. Expanding $\hat{\psi}^\dagger(\mathbf{r}) = \sum_\lambda \psi^*_\lambda(\mathbf{r}) a^\dagger_\lambda$ where $a^\dagger_\lambda$ creates an electron in the single–particle HF state ψ_λ of n electrons, we find

$$\gamma \propto \psi^*_{n+1}(\mathbf{r}) \tag{83}$$

for the $n \to n+1$ transition. This expression is similar to the expression found for the CI model except that the single–particle HF wave function replaces the non–interacting wave function.

We have shown in Section III E that the statistics of the single–particle HF wave functions are the same as in standard RMT. In particular, the distribution of the components $\psi_{n+1}(j)$ of the HF wave function ψ_{n+1} in a fixed basis $|j\rangle$ is given by Eq. (65). For a chaotic ballistic dot such a fixed basis $\chi_j(\mathbf{r})$ is given by the free particle states with energy $\epsilon = \hbar^2 k^2/2m$, e.g., circular waves $\chi_j(\mathbf{r}) \propto J_j(kr) e^{ij\theta}$ ($j = 0, \pm 1, \pm 2 \ldots$) where J_j are Bessel functions of the first kind. A single–particle eigenfunction of the non–interacting dot can be expanded $\psi_\alpha(\mathbf{r}) = \sum_j \psi_\alpha(j) \chi_j(\mathbf{r})$ and, for a chaotic dot, the components $\psi_\alpha(j)$ follow RMT statistics. Expanding the HF wave function ψ_{n+1} in the same basis $\psi_{n+1}(\mathbf{r}) = \sum_j \psi_l(j) \chi_j(\mathbf{r})$, we can view $\psi_{n+1}(\mathbf{r})$ as a projection of ψ_{n+1} on a fixed vector whose components are $\chi_j(\mathbf{r})$. Because of the orthogonal (unitary) invariance of the HF ensemble, such a projection has the same distribution as the distribution (66) of an eigenvector component. Thus the distribution of $\Gamma = |\gamma|^2$ is given by (67) and approaches a Porter–Thomas distribution for large m. Using $\overline{\psi^*_{n+1}(i) \psi_{n+1}(j)} = \delta_{ij}/m$, we also find (see, for example, Section V.B in Ref. 2)

$$\frac{\overline{\gamma^{l^*} \gamma^r}}{\sigma(\gamma^l)\sigma(\gamma^r)} = J_0(k|\mathbf{r_l} - \mathbf{r_r}|) \ , \tag{84}$$

where $\sigma(\gamma)$ is the standard deviation of the partial amplitude γ. Thus the correlation between the left and right partial width amplitudes decays in magnitude as $\sim (k|\mathbf{r}_l - \mathbf{r}_r|)^{-1/2}$, and can be ignored when the distance between the left and right leads is large compared with the Fermi wavelength.

Since Γ^l and Γ^r are uncorrelated and each follows a Porter–Thomas distribution, we conclude (in Koopmans' limit) that the peak–height distribution for the orthogonal (unitary) many–body ensembles of Section II is the same as the distribution derived from standard RMT.

Beyond Koopmans' limit, the single–particle HF wave functions depend on the number of electrons on the dot and are accordingly denoted by $\psi^{(n)}_\lambda$. Expanding in the HF basis of n electrons, $\hat{\psi}^\dagger(\mathbf{r}) = \sum_\lambda \psi^{(n)*}_\lambda(\mathbf{r}) a^\dagger_\lambda$ (where $a^\dagger_\lambda$ creates an electron in $\psi^{(n)}_\lambda$), we find

$$\langle \Phi_{\rm HF}(n+1) | \hat{\psi}^\dagger(\mathbf{r}) | \Phi_{\rm HF}(n) \rangle = (-)^n \sum_{\lambda=n+1}^{m} \psi^{(n)^*}_\lambda(\mathbf{r}) \det A^{(\lambda)}, \tag{85}$$

where $A^{(\lambda)}$ is an $(n+1) \times (n+1)$ matrix defined by $A^{(\lambda)}_{\alpha\beta} = \langle \psi^{(n+1)}_\alpha | \psi^{(n)}_\beta \rangle$ and $A^{(\lambda)}_{\alpha,n+1} = \langle \psi^{(n+1)}_\alpha | \psi^{(n)}_\lambda \rangle$ for $\alpha = 1, \ldots, n+1$; $\beta = 1, \ldots, n$.

An equivalent expression for γ can be derived by rewriting $\gamma \propto \langle \Phi_{\rm HF}(n) | \hat{\psi}(\mathbf{r}) | \Phi_{\rm HF}(n+1) \rangle^*$ and expanding in the HF basis of $n+1$ electrons $\hat{\psi}(\mathbf{r}) = \sum_\lambda \psi^{(n+1)}_\lambda(\mathbf{r}) a_\lambda$ (where now a_λ annihilates an electron in $\psi^{(n+1)}_\lambda$). We find

$$\langle \Phi_{\rm HF}(n+1) | \hat{\psi}^\dagger(\mathbf{r}) | \Phi_{\rm HF}(n) \rangle = \sum_{\lambda=1}^{n+1} (-)^{\lambda-1} \psi^{(n+1)*}_\lambda(\mathbf{r}) \det B^{(\lambda)}, \tag{86}$$

where $B^{(\lambda)}$ is an $n \times n$ matrix defined by $B^{(\lambda)}_{\alpha\beta} = \langle \psi^{(n+1)}_\alpha | \psi^{(n)}_\beta \rangle$ for $\alpha = 1, \ldots, \lambda-1, \lambda+1, \ldots, n+1$ and $\beta = 1, \ldots, n$.

Taking for $\psi^{(n)}_\lambda(\mathbf{r})$ a projection of the HF wave function $\psi^{(n)}_\lambda$ on a fixed vector, we have used Eq. (85) to calculate the distribution of the renormalized partial width $\hat{\Gamma} = \Gamma/\bar{\Gamma}$ in the HF approach (alternatively, we can use Eq. (86) with $\psi^{(n+1)}_\lambda(\mathbf{r})$ given by a projection of the HF wave function $\psi^{(n+1)}_\lambda$). Fig. 16 shows (symbols) the distribution $P(\ln \hat{\Gamma})$ versus $\ln \hat{\Gamma}$ for $u = 0.05, 0.1, 0.15$

and 0.25. The solid line is the distribution (67) for $m = 30$ and the dashed line is the Porter–Thomas distribution. For $u = 0$, only the first (last) term in Eq. (85) (Eq. (86)) differs from zero, and the distribution is given by Eq. (67). As u increases, more terms contribute and the distribution of $\hat{\Gamma}$ gets closer to the Porter–Thomas distribution (this is plausible because of a central–limit theorem). The inset of Fig. 16 shows the average value of Γ in units of the average value of Γ in the CI model. This average value decreases from 1 as u increases. We have also calculated correlations of partial widths (e.g., $(\overline{\Gamma^l\Gamma^r} - \bar{\Gamma}^l\bar{\Gamma}^r)/[\sigma(\Gamma^r)\sigma(\Gamma^l)]$), and found them to be generally weaker than predicted by Eq. (69).

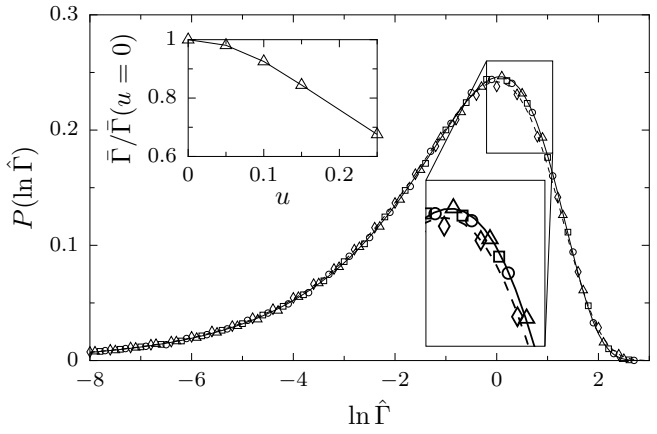

FIG. 16: The distribution $P(\ln\hat{\Gamma})$ versus $\ln\hat{\Gamma}$ where $\hat{\Gamma}$ is the renormalized partial width in the HF approximation. Shown are results for $u = 0.05$ (triangles), 0.1 (squares), 0.15 (circles) and 0.25 (diamonds). We use the ensemble (17) with $m = 30$ and $n = 10$. The solid line is the distribution (67) and the dashed line is the Porter-Thomas distribution. We have magnified a section of the graph to show more details. Inset: $\bar{\Gamma}/\bar{\Gamma}(u = 0)$ versus u.

We conclude that in the HF approach, the partial–width distribution is not affected by the fluctuations of the residual interaction and (in the limit of large m) remains Porter–Thomas like. Consequently, the peak–height distribution is similar to the distribution predicted from standard RMT. The residual interaction only affects the average values of the partial widths.

V. SUMMARY AND CONCLUSION

In this paper we have discussed a generic approach towards the understanding of the statistical properties of an (almost) closed diffusive or chaotic quantum dot in the limit of large but finite Thouless conductance g.

The randomness of the single–particle Hamiltonian of a closed diffusive or chaotic dot induces randomness into the two–body interaction matrix elements when these are expressed in the eigenbasis of the single–particle Hamiltonian. In the first part of this paper we have classified the resulting induced two–body ensembles. These depend on both, the underlying space–time symmetries of the dot, and the symmetries of the interaction matrix elements under permutations of the single–particle basis. Our classification applies to the non–antisymmetrized matrix elements and therefore holds in the presence of spin degrees of freedom. The ensembles for the spinless case follow directly by antisymmetrizing the interaction matrix elements. We have ignored spin–orbit scattering in the dot, so the resulting two–body ensembles have either orthogonal or unitary symmetry depending on whether time–reversal symmetry is conserved or broken. Aside from the symmetries, the ensembles are characterized by three parameters: The mean level spacing Δ due to the random one–body Hamiltonian, the parameter u which measures the fluctuations of the two–body interaction matrix elements, and the number n of electrons on the dot.

The presence of two–body interactions poses difficulties in treating the many–body system. Therefore, in the second part of this work we have used the HF approximation to study generic interaction effects in an (almost) closed dot. The HF approximation is not only tractable, but also allows us to use a single–particle formulation, optimized to include interaction effects.

Applying the HF approximation to the two–body ensembles, we have developed a generic statistical HF approach. In this approach we have solved the HF equations for a large number of realizations of the ensemble, thereby generating a one–body ensemble of single–particle HF energies and wave functions. We have studied the statistical properties of this induced HF one–body ensemble, distinguishing the lowest n filled levels from the remaining empty ones. For both the filled and the empty levels separately, the nearest–neighbor level spacing follows the Wigner distribution. This is not true for the HF gap separating the filled and empty levels. The gap distribution has the form of a convolution of a Wigner distribution with a Gaussian whose width is proportional to u, while the average value of the gap increases quadratically with u (in leading order). By studying a suitable spacing correlator, we have found that the gap weakens the correlation between filled and empty levels, but similar correlators within the filled or empty levels separately continue to follow RMT. We have shown that the single–particle HF ensemble satisfies orthogonal (unitary) invariance in the presence (absence) of time-reversal symmetry. Consequently the HF wave function components (in a fixed basis) satisfy RMT statistics. We have also studied the statistics of the interaction matrix elements in the HF basis (which reflect the statistical properties of the HF wave functions). The distributions of the HF matrix elements are Gaussian and, thus, can be characterized by their first two moments. The average of a diagonal interaction matrix element acquires a u^2 correction. The value of that correction depends on whether

the corresponding single–particle orbitals are both filled, both empty, or whether one is filled, the other, empty. The variances, on the other hand, remain close to their values in the non–interacting basis.

The HF ensemble can be used to study the statistical properties of various observables. In particular, we have studied the generic properties of the peak–spacing distribution and of the peak–height distribution. A simple interpretation of the results is provided in Koopmans' limit where it is assumed that the HF wave functions do not change upon the addition of an electron to the dot. The peak–spacing distribution is well approximated by a convolution of a Wigner distribution with a Gaussian whose width is the standard deviation of a diagonal interaction matrix element. The peak–height distribution, on the other hand, is found to be insensitive to the residual interactions.

We have confined ourselves to the HF approximation for spinless electrons. The presence of spin leads to additional technical difficulties in a mean–field approach. In particular, only the z–component of total spin (but not total spin itself) is conserved. Because of this restriction in our calculations, it is not possible to make a quantitative comparison between our results and experiment. In the presence of spin, the single–particle levels are doubly degenerate. Therefore, the peak–spacing distribution is expected to be bimodal. The exchange interaction associated with the spin degrees of freedom explains the finite–temperature suppression of the width of the peak–spacing distribution,[15] but at low temperatures the distribution is expected to remain bimodal. No such bimodality is observed in the experiments, however. This fact is related to the fluctuating part of the interaction (which is of order $u \propto \Delta/g$). We have seen that in the spinless case, these fluctuations affect the shape of the peak–spacing distribution and lead to a distribution which is intermediate between a Wigner distribution and a Gaussian distribution, in qualitative agreement with experiments. It would be interesting to study the corresponding finite–g effects in the presence of spin, using the HF approximation within the induced two–body ensembles discussed in Section II. This should lead to a generic peak–spacing distribution that can be directly compared with the experimental data. As for the peak–height distribution, RMT plus exchange interaction (without the fluctuating part of the interaction) were found to provide a quantitative description of the observed features at low temperatures.[15,40] We have shown here that in the absence of spin, the peak–height distribution is insensitive to the fluctuating residual interaction. If this conclusion continues to hold in the presence of spin, it will fully explain the observed low–temperature peak–height distribution. A definitive answer could be provided using the induced two-body ensembles of Section II that include spin.

Acknowledgments

We thank Y. Gefen, Ph. Jacquod, L. Kaplan and A.D. Mirlin for useful discussions. This work was supported in part by the U.S. DOE grant No. DE-FG-0291-ER-40608. Y.A. would like to acknowledge support by a von Humboldt Senior Scientist Award and the hospitality of the Max-Planck-Institut für Kernphysik at Heidelberg where part of this work was completed. A.W. acknowledges support by the SFB 484.

[1] T. Guhr, A. Müller-Groeling, and H. A. Weidenmüller, Phys. Rep. **299**, 190 (1998).
[2] Y. Alhassid, Rev. Mod. Phys. **72**, 895 (2000).
[3] R.A. Jalabert, A.D. Stone, and Y. Alhassid, Phys. Rev. Lett. **68**, 3468 (1992).
[4] Y. Alhassid and H. Attias, Phys. Rev. Lett. **76**, 1711 (1996).
[5] U. Sivan, R. Berkovits, Y. Aloni, O. Prus, A. Auerbach, and G. Ben-Yoseph, Phys. Rev. Lett. **77**, 1123 (1996).
[6] F. Simmel, T. Heinzel and D.A. Wharam, Europhys. Lett. **38**, 123 (1997).
[7] S. R. Patel, S. M. Cronenwett, D. R. Stewart, A. G. Huibers, C. M. Marcus, C. I. Duruöz, J. S. Harris, Jr., K. Campman, and A. C. Gossard, Phys. Rev. Lett. **80**, 4522 (1998).
[8] S. Lüscher, T. Heinzel, K. Ensslin, W. Wegscheider, and M. Bichler, Phys. Rev. Lett. **86**, 2118 (2001).
[9] Ya. M. Blanter, A.D. Mirlin, and B.A. Muzykantskii, Phys. Rev. Lett. **78**, 2449 (1997).
[10] R. Berkovits, Phys. Rev. Lett. **81**, 2128 (1998).
[11] A.D. Mirlin, Phys. Rep. **326**, 260 (2000).
[12] I.L. Kurland, I.L. Aleiner, and B.L. Altshuler, Phys. Rev. B **62**, 14886 (2000).
[13] I.L. Aleiner, P.W. Brouwer, and L.I. Glazman, Phys. Rep. **358**, 309 (2002).
[14] G. Usaj and H.U. Baranger, Phys. Rev. B **64**, 201319(R) (2001).
[15] Y. Alhassid and T. Rupp, Phys. Rev. Lett. **91**, 056801 (2003).
[16] Y. Alhassid and S. Malhotra, Phys. Rev. B **66**, 245313 (2002).
[17] G. Usaj and H. U. Baranger, Phys. Rev. B **66**, 155333 (2002).
[18] A. Cohen, K. Richter, and R. Berkovits, Phys. Rev. B **60**, 2536 (1999).
[19] P.N. Walker, G. Montambaux, and Y. Gefen, Phys. Rev. B **60**, 2541 (1999).
[20] S. Levit and D. Orgad, Phys. Rev. B **60**, 5549 (1999).
[21] K. Hirose, F. Zhou, and N.S. Wingreen, Phys. Rev. B **63**, 075301 (2001).
[22] K. Hirose and N.S. Wingreen, Phys. Rev. B **65**, 193305 (2002).
[23] H. Jiang, H. U. Baranger, and W. Yang, Phys. Rev. Lett. **90**, 026806 (2003)
[24] K.K. Mon and J.B. French, Ann. Phys. (N.Y.) **95**, 90 (1975).

[25] J.B. French and S.S.M. Wong, Phys. Lett. B **33**, 449 (1970); **35**, 5(1971).
[26] O. Bohigas and J. Flores, Phys. Lett. B **4**, 261 (1971); **35**, 383 (1971).
[27] L. Benet, T. Rupp, and H. A. Weidenmüller, Ann. Phys. **292**, 67 (2001).
[28] L. Benet and H.A. Weidenmüller, J. Phys. A **36**, 3569 (2003).
[29] Y. Alhassid, Ph. Jacquod, and A. Wobst, Phys. Rev. B **61**, 13357R (2000).
[30] Y. Alhassid and A. Wobst, Phys. Rev. B **65**, 041304R (2002).
[31] Ph. Jacquod and A.D. Stone, Phys. Rev. Lett. **84**, 3938 (2000); Phys. Rev. B **64** 214416 (2001).
[32] L. Kaplan, T. Papenbrock, and C.W. Johnson, Phys. Rev. C **63**, 014307 (2001).
[33] T. Koopmans, Physica (Amsterdam) **1**, 104 (1934).
[34] K.B. Efetov, Adv. Phys. **32**, 53 (1983).
[35] A.D. Mirlin, private communication.
[36] Y. Alhassid and Y. Gefen, cond-mat/0101461.
[37] Ya. M. Blanter, A.D. Mirlin, and B.A. Muzykantskii, Phys. Rev. B **63**, 235315 (2001).
[38] T.A. Brody, J. Flores, J.B. French, P.A. Mello, A. Pandey, and S.S.M. Wong, Rev. Mod. Phys. **53**, 385 (1981).
[39] R. Berkovits and U. Sivan, Europhys. Lett. **41**, 653 (1998).
[40] G. Usaj and H. U. Baranger, Phys. Rev. B **67**, 121308R (2003)